Effects of Ultraviolet Modification on the Gating Energetics of Cyclic Nucleotide–gated Channels

Thomas R. Middendorf*‡ and Richard W. Aldrich‡

From the *Neurobiology Department, and ‡Department of Molecular and Cellular Physiology, and Howard Hughes Medical Institute, School of Medicine, Stanford University, Stanford, California 94305

abstract Middendorf et al. (Middendorf, T.R., R.W. Aldrich, and D.A. Baylor. 2000. *J. Gen. Physiol.* 116:227–252) showed that ultraviolet light decreases the current through cloned cyclic nucleotide–gated channels from bovine retina activated by high concentrations of cGMP. Here we probe the mechanism of the current reduction. The channels' open probability before irradiation, $P_o(0)$, determined the sign of the change in current amplitude that occurred upon irradiation. UV always decreased the current through channels with high initial open probabilities [$P_o(0) > 0.3$]. Manipulations that promoted channel opening antagonized the current reduction by UV. In contrast, UV always increased the current through channels with low initial open probabilities [$P_o(0) \leq 0.02$], and the magnitude of the current increase varied inversely with $P_o(0)$. The dual effects of UV on channel currents and the correlation of both effects with $P_o(0)$ suggest that the channels contain two distinct classes of UV target residues whose photochemical modification exerts opposing effects on channel gating. We present a simple model based on this idea that accounts quantitatively for the UV effects on the currents and provides estimates for the photochemical quantum yields and free energy costs of modifying the UV targets. Simulations indicate that UV modification may be used to produce and quantify large changes in channel gating energetics in regimes where the associated changes in open probability are not measurable by existing techniques.

key words: cyclic guanine monophosphate • electrophysiology • ligand-gated channel • ion channel gating • ultraviolet light

INTRODUCTION

Cyclic nucleotide-gated (CNG)[1] ion channels are activated cooperatively by the binding of multiple cyclic nucleotide ligands to a cytoplasmic COOH-terminal domain of the protein (Kaupp et al., 1989). CNG channels play central roles in vision (Stryer, 1986; Yau and Baylor, 1989), olfaction (Lancet, 1986; Zufall et al., 1994), and possibly other sensory modalities (Coburn and Bargmann, 1996; Komatsu et al., 1996; Misaka et al., 1998). Their expression in a host of other tissues, including heart (Biel et al., 1994; Ratcliffe et al., 1995), testis (Biel et al., 1994; Weyand et al., 1994), kidney (Marunaka et al., 1991; Ahmad et al., 1992; Biel et al., 1994; Karlson et al., 1995), and brain (Yao et al., 1995; Kingston et al., 1996; Ding et al., 1997; Zhang et al., 1997; Timpe et al., 1999), suggests that they may participate in nonsensory processes as well. Understanding the molecular mechanism of CNG channel activation is of interest not only due to the channels' important physiological roles, but also because they serve as a model system for studying allostery and cooperativity.

The primary experiment used to test activation models for CNG and other ligand-gated channels is to measure the dependence of their open probability on cyclic nucleotide concentration. The endpoints of this dose–response relation are often difficult to measure accurately because the open probabilities of CNG channels span the enormous range from $<10^{-5}$ in the absence of ligand (Ruiz and Karpen, 1997; Tibbs et al., 1997) to >0.90 in saturating ligand (Goulding et al., 1994; Taylor and Baylor, 1995; Varnum and Zagotta, 1996). Furthermore, two other defining features of the ligand dose–response relation for these channels, the apparent slope and the concentration of cyclic nucleotide producing half-maximal activation, may vary significantly between experiments (Ruiz et al., 1999). The combined effect of these uncertainties is to limit the usefulness of the dose–response relation in evaluating theories for CNG channel gating.

Combined measurements of gating and ionic currents have greatly assisted the process of discriminating among candidate models for the voltage-dependent activation of *Shaker* potassium channels (Bezanilla et al., 1994; Zagotta et al., 1994; Schoppa and Sigworth, 1998). Likewise, detailed models for the activation of large conductance, Ca^{+2}-activated K^+ (*mSlo*) channels have been developed using measurements of the chan-

Address correspondence to Richard W. Aldrich, Department of Molecular and Cellular Physiology, Howard Hughes Medical Institute, Stanford University, Stanford, CA 94305. Fax: 650-725-4463; E-mail: raldrich@leland.stanford.edu

[1]*Abbreviations used in this paper:* CD model, coupled dimer model; CNG, cyclic nucleotide-gated; HH model, Hodgkin-Huxley model; MWC model, Monod-Wyman-Changeux model; OLF channel, rat olfactory CNG channel; RET channel, bovine retinal CNG channel.

nels' sensitivity to both membrane voltage and intracellular Ca^{2+} concentration (Cox et al., 1997; Cui et al., 1997; Horrigan and Aldrich, 1999; Horrigan et al., 1999; Rothberg and Magleby, 1999). In this spirit, perturbations of gating energetics combined with measurements of the ligand dose–response relation may be useful for studying the activation mechanism of CNG channels and other ligand-gated channels that are relatively insensitive to membrane voltage.

Spectroscopic methods offer a promising approach for supplementing the information obtained from traditional electrical measurements on channels. For example, luminescence signals from voltage-gated channels labeled with fluorescent dyes have revealed new details about the protein motions involved in gating (Mannuzzu et al., 1996; Cha and Bezanilla, 1997; Cha et al., 1999; Glauner et al., 1999). We have used a complementary spectroscopic approach that employs UV light to photochemically modify the intrinsic aromatic amino acid chromophores in CNG channels. The preceding paper (Middendorf et al., 2000) showed that UV dramatically reduces the ionic currents through fully liganded CNG channels. The wavelength dependence of the effect was very similar to the absorption spectrum of tryptophan, suggesting that UV decreased the currents by photochemically modifying one or more "target" tryptophan residues in the channels. Here we investigate the mechanism of the UV effect on the currents.

MATERIALS AND METHODS

Channel expression, electrical recordings, solutions, and UV irradiation apparatus were described in the preceding paper (Middendorf et al., 2000). Briefly, channels were expressed in *Xenopus* oocytes by microinjection of the appropriate cRNA. Currents through inside-out membrane patches excised from injected oocytes were recorded 3–21 d after injection. Patches were irradiated with light emitted by a 75 W xenon arc lamp and focused on the preparation with a quartz lens. UV wavelengths were selected using 10-nm full-width at half-maximum bandpass interference filters. The cDNA for the rat olfactory (OLF) CNG channel was a generous gift from Prof. R. Reed of Johns Hopkins University (Baltimore, MD).

RESULTS

Effect of UV on Ligand Dose–Response Relation

As shown previously (Middendorf et al., 2000), UV decreased the amplitude of macroscopic currents through bovine retinal CNG (RET) channels activated by a saturating concentration of cGMP (1 mM, Fig. 1 A). Since cyclic nucleotides absorb strongly at the UV wavelengths employed (250–330 nm), the patches were irradiated in the absence of cGMP to avoid possible photochemical modification of the ligand or its cross linking to the channels.

In stark contrast to the current reduction in 1 mM cGMP (Fig. 1 A), the same UV exposures increased the current activated by a low concentration of cGMP (2 μM, B). Each trace was corrected for leak by subtracting the current in the absence of cGMP after the same UV dose. This procedure ruled out the trivial possibilities that the additional current after irradiation flowed through the leakage conductance of the seal or through the UV-activated conductance (Middendorf et

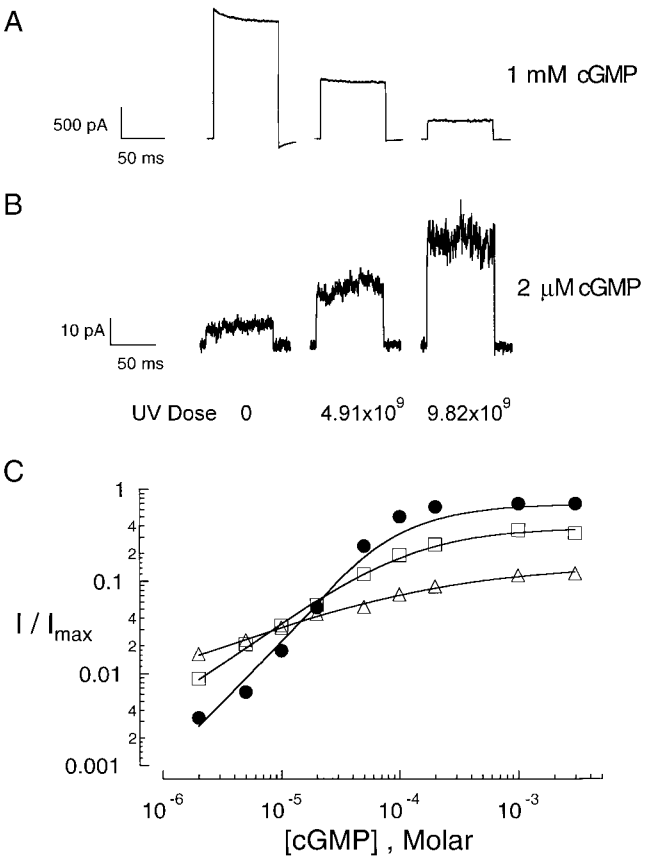

Figure 1. Effect of UV light on currents through RET channels activated by saturating and low concentrations of ligand. (A and B) Current in response to 0 to +50 mV potential steps in the presence of: (A) saturating (1 mM) cGMP, and (B) 2 μM cGMP. Cyclic GMP-dependent current amplitudes before UV and after cumulative doses of 4.91 and 9.82 × 10^9 photons · μm^{-2} were: for 1 mM cGMP: 2,110 ± 4, 980 ± 5, and 297 ± 9 pA; and for 2 μM cGMP: 7 ± 2, 22 ± 3, and 40 ± 4 pA. Note the difference in vertical scales for traces in A and B, which are from the same patch. (C) Effect of UV light on RET channel cGMP dose–response relation. The cGMP-activated current (I) divided by the maximal current in 1 mM cGMP before irradiation (I_{max})is plotted as a function of cyclic GMP concentration on double logarithmic coordinates. Relations were measured before UV exposure (●), and after cumulative doses of 4.91 × 10^9 photons · μm^{-2} (□), and 9.82 × 10^9 photons · μm^{-2} (△). The continuous curves show fits to the results using the Hill equation (Eq. 1 of the text). The Hill coefficient, *h*, and the apparent affinity, $K_{1/2}$, were: before UV exposure, h = 1.85 and $K_{1/2}$ = 70.2 μM; after 4.91 × 10^9 photons · μm^{-2}, h = 0.97 and $K_{1/2}$ = 125 μM; after 9.82 × 10^9 photons · μm^{-2}, h = 0.53 and $K_{1/2}$ = 149 μM. Results from same patch as in A and B. The patch was irradiated with 280 nm UV in the absence of cGMP. The light intensity at the patch was 1.96 × 10^8 photons · μm^{-2} · s^{-1}.

al., 2000), since these conductances were insensitive to cGMP (data not shown).

Fig. 1 C displays the combined results for the patch in A and B as a series of pre- and post-UV ligand dose–response relations. These relations plot the fractional current activation I/I_{max} (defined as the current relative to the maximal current in saturating cGMP before irradiation) as a function of cGMP concentration. The relations crossed at $I/I_{max} \approx 0.04$ due to the opposite effects of UV on the currents activated by high and low concentrations of cGMP. This fractional activation occurred at a cGMP concentration of ~15 μM, which is 4.7× lower than the initial half-saturating concentration of 70.2 μM. The slopes of the relations and their positions on the abscissa were compared by fitting them with the Hill equation:

$$\frac{I(D)}{I_{max}(0)} = \frac{I_{max}(D)}{I_{max}(0)} \cdot \frac{[cGMP]^h}{[cGMP]^h + (K_{1/2})^h}, \quad (1)$$

where $I_{max}(D)$ is the maximal current in saturating ligand after a UV dose D, h is the Hill coefficient, and $K_{1/2}$ is the half-saturating ligand concentration. The Hill coefficient decreased progressively from 1.85 before UV to 0.97 and 0.53 after the first and second UV doses, respectively. Higher UV doses reduced the fractional activation even further in other experiments (Middendorf et al., 2000), suggesting that the Hill coefficient for fully modified channels may be <0.53. Furthermore, the curves may be artificially steepened because the leak correction procedure may have overestimated the leak at low cGMP concentrations due to the increased spontaneous channel openings after UV (see Fig. 15). The Hill coefficients for the post-UV relations are difficult to interpret, however, since the patches likely contained a mixture of channels with different numbers of modified target residues. The reduced slope of the overall relation for such a heterogeneous population could result from UV effects on $K_{1/2}$ rather than h. UV had similar effects on the cGMP dose–response relations of RET channels from two other patches.

We also investigated the effect of UV on currents through a second type of CNG channel from rat olfactory epithelium (denoted OLF) (Dhallan et al., 1990). The open probability (Gordon and Zagotta, 1995b; Varnum and Zagotta, 1996) and single channel conductance (Kaupp et al., 1989; Goulding et al., 1992) of OLF channels are larger than those of RET channels. The amino acid sequences of OLF and RET channels are similar, with most of the differences occurring outside of the "core" region that contains the six presumed membrane-spanning domains and the cyclic nucleotide–binding domain. 8 of the 10 tryptophan residues occupy equivalent positions in RET and OLF channel subunits. OLF and RET channels contain nonequivalent tryptophans in the cytoplasmic NH_2-terminal domain before the first presumed transmembrane segment (W81 in OLF and W9 in RET). In addition, OLF channels contain a tryptophan in the S1 transmembrane segment, W141, that is not present in RET channels, while RET channels contain a tryptophan in the S3–S4 linker, W263, that is not found in OLF channels.

The effects of UV light on OLF channels (Fig. 2) were similar in several respects to those on RET channels (Fig. 1). UV decreased the current through OLF channels activated by saturating cGMP (1 mM, Fig. 2 A), but increased the current activated by a very low concentration of cGMP (0.2 μM, Fig. 2 B) in the same patch after the identical doses. In addition, UV decreased the slope of the cGMP dose–response relation for OLF channels (Fig. 2 C). The relations before and after UV crossed at $I/I_{max} \approx 0.03$, corresponding to 0.5 μM cGMP (5.6× lower than the initial half-saturating concentration of 2.8 μM).

OLF and RET channels differed in their absolute sensitivity to UV. A dose of 4.91×10^9 photons · μm^{-2} at 280 nm reduced the amplitude of currents through RET channels in saturating cGMP by a large factor ($I/I_{max} = 0.464 \pm 0.003$, Fig. 1), but had only a slight effect on the current through OLF channels ($I/I_{max} = 0.944 \pm 0.003$, Fig. 2). The reason for the difference in UV sensitivities is discussed later (see Fig. 5).

Mechanism of UV Effect

The results in Figs. 1 and 2 are inconsistent with an "all-or-none" effect of UV on CNG channel currents. Models of this type assume that UV has no effect on a channel until modification of a critical number of target residues renders the channel nonconducting (Middendorf et al., 2000). For such a model, only two functionally distinguishable classes of channels are possible: channels containing less than the critical number (n^*) of modified target residues that are functionally identical to unmodified channels, and channels that contain at least n^* modified targets that do not conduct current. Thus, photochemical modification simply reduces the number of functional channels in the patch, and UV is predicted to reduce the current by a constant factor at all ligand concentrations. This prediction is inconsistent with the results in Figs. 1 and 2. The preceding paper (Middendorf et al., 2000) showed that the difference in UV sensitivities of wild-type and W353Y mutant RET channels is also inconsistent with an all-or-none UV effect. We conclude that UV reduces CNG channel currents in a graded fashion, and that some UV-modified channels conduct current, but their ligand dose–response relations differ from those of unmodified channels.

What parameters of channel activation are changed by UV? The current through a membrane patch containing N channels is given by Eq. 2:

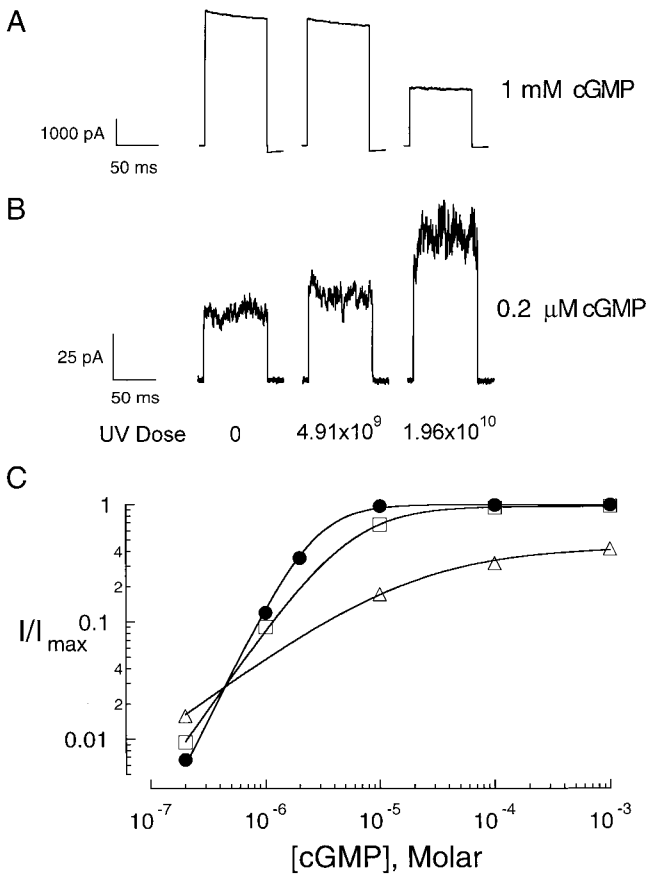

Figure 2. Effect of UV light on currents through rat olfactory CNG (OLF) channels activated by saturating and low concentrations of ligand. (A and B) Currents in response to potential steps from 0 to +50 mV in the presence of (A) saturating (1 mM) cGMP, and (B) 0.2 μM cGMP. Cyclic GMP–dependent current amplitudes before UV and after cumulative doses of 4.91×10^9 and 1.96×10^{10} photons · μm^{-2} were: for 1 mM cGMP: 5,187 ± 12, 4,899 ± 9, and 2,210 ± 5 pA; and for 0.2 μM cGMP: 36.8 ± 3.3, 46.0 ± 4.0, and 80 ± 7 pA. Note the difference in vertical scales for traces in A and B, which are from the same patch. (C) Effect of UV light on OLF channel cGMP dose–response relation. The cGMP-activated current before UV exposure (●), and after cumulative doses of 4.91×10^9 (□) and 1.96×10^{10} (△) photons · μm^{-2}, divided by the maximal current in 1 mM cGMP before irradiation, are plotted as a function of cGMP concentration on double logarithmic coordinates. The continuous curves show fits to the results using the Hill equation (Eq. 1). The Hill coefficient, h, and the half-saturating cGMP concentration, $K_{1/2}$, were: before UV exposure, $h = 1.90$ and $K_{1/2} = 2.81$ μM; after 4.91×10^9 photons · μm^{-2}, $h = 1.44$ and $K_{1/2} = 4.87$ μM; and after 96×10^{10} photons · μm^{-2}, $h = 0.72$ and $K_{1/2} = 18.7$ μM. Results are from same patch as in A and B. The patch was irradiated with 280 nm UV in the absence of cGMP.

$$I = NP_o i_{sc}, \quad (2)$$

where i_{sc} is the current through a single open channel. We assume that UV does not alter N, the total number of channels initially in the patch, and treat "destruction" of channels by UV as a reduction of P_o and/or i_{sc} to zero (see below). The channels' cyclic nucleotide affinity, K_b, also influences the current amplitude, since P_o and i_{sc} depend on the number of bound ligands (Ildefonse and Bennett, 1991; Taylor and Baylor, 1995; Ruiz and Karpen, 1997, 1999; Liu et al., 1998). A priori, UV might alter the channel current by altering any combination of the parameters P_o, i_{sc}, and K_b. The opposite effects of UV on the currents through channels activated by high versus low concentrations of cGMP (Figs. 1 and 2) are inconsistent with a single effect of UV on these parameters. We conclude that UV exerts at least two distinct effects on the channels, and consider first the mechanism of the current reduction in saturating cGMP.

Mechanism of Current Reduction by UV

UV might have decreased the currents through CNG channels activated by 1 mM cGMP (Figs. 1 A and 2 A) by reducing the channels' affinity for ligand such that 1 mM cGMP was no longer saturating. However, raising the cGMP concentration from 1 to 3 mM did not increase the current amplitude after irradiation (Fig. 1). In other experiments (data not shown), raising the cGMP concentration from 1 to 20 mM did not increase the post-UV current amplitude. The UV effects on OLF channels (Fig. 2 C) were also inconsistent with this mechanism, since the current amplitude after irradiation saturated at ~40% of the pre-UV value.

If UV altered the channels' unitary conductance, but not their open probability, then UV should reduce the currents activated by any saturating concentration of ligand by the same fraction. In contrast to this prediction, the UV dose–response relations differed for OLF channels activated by 10, 100, and 1,000 μM cGMP (Fig. 3 A), saturating concentrations before irradiation (Fig. 2 C). Increasing the cGMP concentration over this range shifted the relations to the right on the abscissa and increased their slope (Fig. 3 B). The results in Fig. 3 are thus inconsistent with the idea that UV reduced the currents mainly by decreasing the channels' unitary conductance.

The continuous curves in Fig. 3 A are fits to the UV dose–response relations using the all-or-none model of the preceding paper (Middendorf et al., 2000):

$$\frac{I(D)}{I(0)} = 1 - [1 - \exp(-\sigma\phi D)]^{n^*}. \quad (3)$$

The parameter σ in Eq. 3 is the absorption cross section of a UV target, and ϕ is its photochemical quantum yield (the fraction of absorptions that produce a photoproduct). The slope factor, n^*, is a parameter that characterizes the steepness of the UV dose–response relation. No physical significance was attached to the values of these fitting parameters since, as noted above, UV did not alter the currents in an all-or-none manner. Rather, the fits provided a simple means for quantifying

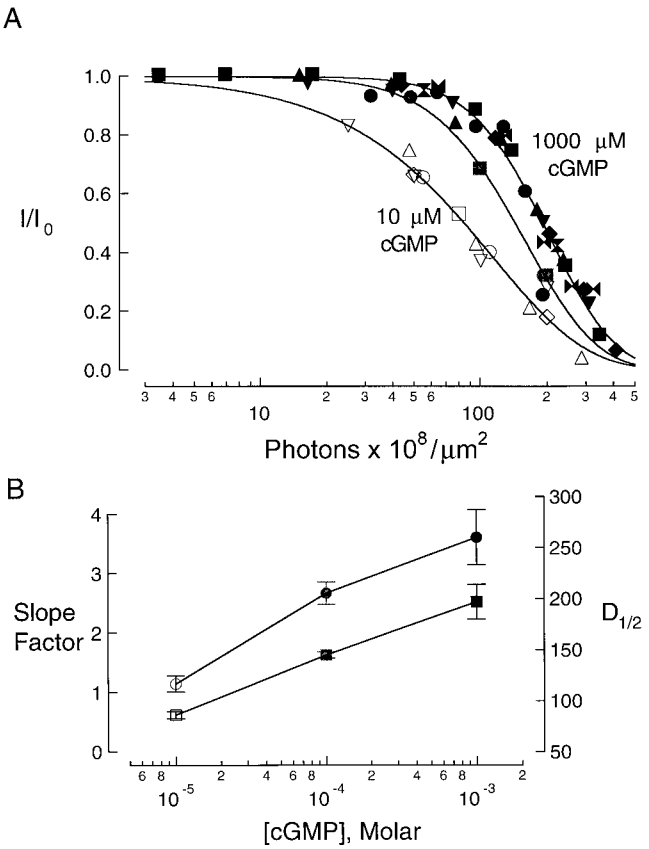

Figure 3. UV effect on OLF channels activated by different, initially saturating cGMP concentrations. (A) UV dose–response relations for OLF channels activated by 10 μM cGMP (open symbols, five experiments), 100 μM cGMP (gray symbols, two experiments), and 1,000 μM cGMP (black symbols, seven experiments). $D_{1/2}$, the UV dose that reduced the current amplitude to one half its initial value, was estimated for each experiment by fitting the UV dose–response relation with the all-or-none model (Eq. 3). The points from each experiment were then shifted along the abscissa so that the $D_{1/2}$ value of the shifted results was equal to the average $D_{1/2}$ value of the unshifted results for all experiments at the same cGMP concentration. Different symbols represent separate experiments. Continuous curves are fits to the pooled results for each concentration using Eq. 3. Patches were irradiated with 280 nm UV in the absence of cGMP. (B) Half-maximal UV dose in photons $\times 10^8 \cdot \mu m^{-2}$, (squares), and slope factor (circles) from the fits in A, plotted as a function of cGMP concentration. The UV parameters are listed in Table I.

the slope of a relation and its $D_{1/2}$ value. The latter quantity is defined as the UV dose that reduced the current amplitude to half of its initial value. The UV parameters obtained from the fits are compiled in Table I.

The results in Fig. 3 are not explained by differential UV effects on the unitary conductances of channel subconductance states. In RET channels, fully liganded channels reside almost exclusively in the level with the largest conductance (Ildefonse and Bennett, 1991; Taylor and Baylor, 1995; Ruiz and Karpen, 1997, 1999). Also, results from the preceding paper (Middendorf et al., 2000) indicate that UV does not affect other pore properties of the channels, such as their ion selectivity. These results do not completely rule out UV effects on i_{sc}; however, results to be presented indicate that possible effects of this type are small. Having ruled out other possibilities, we conclude that UV reduced the currents mainly by lowering the channels' open probability.

It was not possible to measure directly the effect of UV on the unitary conductance and open probability of single CNG channels because of interference by the UV-activated conductances in oocytes (Middendorf et al., 2000). Therefore, we used the alternate approach of modeling the UV effect on macroscopic currents (see below).

Energy Additive Model

Of the various physical models considered in the preceding paper (Middendorf et al., 2000), only the energy additive model is consistent with the graded reduction in channel open probability suggested by the results in Figs. 1–3. This model was described in detail previously (Middendorf et al., 2000) and is briefly summarized here.

Assume that fully liganded channels have a single open and a single closed state, contain n identical and independent UV target residues per subunit, and that modification of each target alters the free energy difference between the channels' open and closed states by an equal and additive amount. Then, due to the statistical nature of light absorption, the various channels in a patch will contain different numbers of modified target residues (denoted by the index k) after exposure to a subsaturating UV dose. The equilibrium constant between the open and closed states of a channel with k modified targets, $K(k)$, is given by:

$$K(k) = \exp\{-[\Delta G^0(0) + k \cdot \Delta\Delta G^0(1)]\}. \quad (4)$$

Here, $\Delta G^0(0)$ is the standard free energy difference between channel states before irradiation, and $\Delta\Delta G^0(1)$ is the free energy "cost" of modifying a single target residue. Eq. 4 is simplified by expressing these thermodynamic parameters in RT units (R is the gas constant, T is the absolute temperature, and $RT = 0.58$ kcal/mol). The equilibrium constant is related to the channels' open probability according to

$$K(k) = \frac{P_o(k)}{1 - P_o(k)}. \quad (5)$$

Since irradiation decreases P_o, modification of the UV targets favors channel closing (i.e., $\Delta\Delta G^0(1) > 0$).

The energy additive model is illustrated by the schematic in Fig. 4 A. Before irradiation, the open state O_0 has a lower free energy than the closed state C_0, consis-

TABLE I

UV Sensitivity Parameters

Channel	Ligand	Concentration	$D_{1/2}$	Relative UV sensitivity	Slope factor	*m*
		μM	*photons · μm*$^{-2}$			
RET	cGMP	1000	$(4.58 \pm 0.30) \times 10^9$	1.00 ± 0.09	1.39 ± 0.05	10
RET	cGMP	100	$(3.84 \pm 0.39) \times 10^9$	1.19 ± 0.14	1.21 ± 0.05	6
RET	cGMP	1000*	$(9.16 \pm 0.27) \times 10^9$	0.50 ± 0.04	1.89 ± 0.09	3
RET	cAMP	10000*	$(5.29 \pm 0.16) \times 10^9$	0.87 ± 0.06	1.12 ± 0.03	3
OLF	cGMP	1000	$(1.97 \pm 0.17) \times 10^{10}$	0.23 ± 0.03	3.59 ± 0.30	7
OLF	cGMP	100	$(1.45 \pm 0.03) \times 10^{10}$	0.32 ± 0.02	2.67 ± 0.19	3
OLF	cGMP	10	$(8.62 \pm 0.33) \times 10^9$	0.53 ± 0.04	1.15 ± 0.13	5
OLF	cAMP	2000	$(1.45 \pm 0.25) \times 10^{10}$	0.32 ± 0.06	2.30 ± 0.17	3
OLF/W332Y	cGMP	1000	$(3.18 \pm 0.29) \times 10^9$	1.44 ± 0.17	1.37 ± 0.10	8
OLF/W332Y	cAMP	1000	$(1.59 \pm 0.19) \times 10^9$	2.88 ± 0.39	1.13 ± 0.13	3
OLF/W332H	cGMP	1000	$(2.56 \pm 0.21) \times 10^9$	1.79 ± 0.19	0.86 ± 0.09	5
OLF/W332H	cAMP	1000	$(1.57 \pm 0.31) \times 10^9$	2.92 ± 0.61	0.65 ± 0.05	3

Summary of UV parameters for CNG channels. $D_{1/2}$ (mean ± SEM) is the photon dose required to reduce the current amplitude to one half its pre-UV value. The relative UV sensitivities, defined as the reciprocals of the $D_{1/2}$ values, are normalized to the UV sensitivity of RET channels activated by 1,000 μM cGMP. The slope factor (mean ± SD) characterizes the maximum steepness of the UV dose–response relations. The $D_{1/2}$ values and slope factors for the UV dose-response relations were quantified by fitting the results using Eq. 3 of the text. *m*, number of separate experiments for each channel/ligand combination. *UV sensitivity was measured in the presence of 10 μM cytoplasmic Ni^{2+}. The light source was a 75 W xenon arc lamp. Patches were irradiated at 280 nm in the absence of cyclic nucleotides.

tent with the high initial open probabilities of RET and OLF channels in saturating cGMP (Table II). The relative free energies of these states must invert after irradiation, since UV ultimately reduces P_o to a value <0.5 (Figs. 1–3). UV may invert the levels by stabilizing or destabilizing either or both states; the observed reduction in P_o requires only a net stabilization of the closed state relative to the open state. For simplicity, the entire effect of UV is represented in Fig. 4 A by an increase in the free energy of the open state.

The current varies with dose according to Eq. 40 of Middendorf et al. (2000):

$$\frac{I(D)}{I(0)} = \sum_{k=0}^{4n} f(k, D) \frac{1 + \exp[\Delta G^0(0)]}{1 + \exp[\Delta G^0(0) + k \cdot \Delta\Delta G^0(1)]}. \quad (6)$$

where $f(k, D)$ denotes the fraction of channels containing k modified target residues after a UV dose *D*:

$$f(k, D) = \binom{4n}{k} [\exp(-\sigma\phi D)]^{(4n-k)} [1-\exp(-\sigma\phi D)]^k. \quad (7)$$

The first term in brackets in Eq. 7 is the appropriate binomial coefficient, σ is the absorption cross section of a target residue, and ϕ is its photochemical quantum yield.

The UV dose–response relation (Eq. 6) depends on five parameters: (a) the absorption cross-section of the target residues, σ; (b) the photochemical quantum yield of the targets, ϕ; (c) the number of target residues per channel subunit, *n*; (d) the free energy difference between the channels' open and closed states before irradiation, $\Delta G^0(0)$; and (e) the free energy cost of modifying a single target residue, $\Delta\Delta G^0(1)$. Ranges of possible parameter values are estimated in the following. (a) The main target residues in RET channels were identified as tryptophans from the close correspondence between the channels' action spectrum and the absorption spectrum of tryptophan (Middendorf et al., 2000). Since tryptophan's absorption cross section is not very sensitive to environment (McLaren and Shugar, 1964), we use the value for tryptophan in free solution, $\sigma = 2.17 \times 10^{-17}$ cm^2 (Middendorf et al.,

TABLE II

CNG Channel Activation Parameters

Channel	Ligand*	P_o	*K*	ΔG^0(*RT*)	Reference
RET	cGMP	0.952	2.0×10^1	−3.0	1–3
RET	cAMP	0.0196	2.0×10^{-2}	+3.9	1–3
RET	cGMP‡	0.9996	2.5×10^3	−7.8	1, 4
RET	cAMP‡	0.82	4.6×10^0	−1.5	1, 4
RET	none	6.8×10^{-6}	6.8×10^{-6}	+11.9	5
OLF	cGMP	0.99995	2.0×10^4	−9.9	1, 6
OLF	cAMP	0.990	1.0×10^2	−4.6	1, 6
OLF	none	9.2×10^{-4}	9.2×10^{-4}	+7.0	1

Summary of CNG channel activation parameters for a variety of experimental conditions. The equilibrium constant for channel opening (*K*) and the free energy difference between open and closed channel states (ΔG^0) were computed from the corresponding open probabilities using Eqs. 4 and 5. *Activation parameters were estimated for channels activated by a saturating concentration of ligand or in the absence of ligand. ‡10 μM cytoplasmic Ni^{2+} was present. References: (1) open probability was determined by us and is in good agreement with results from the following other references: (2) Varnum and Zagotta, 1996; (3) Goulding et. al., 1994; (4) Gordon and Zagotta, 1995a; (5) Ruiz and Karpen, 1997; and (6) Gordon and Zagotta, 1995b. *RT* = 0.58 kcal/mol.

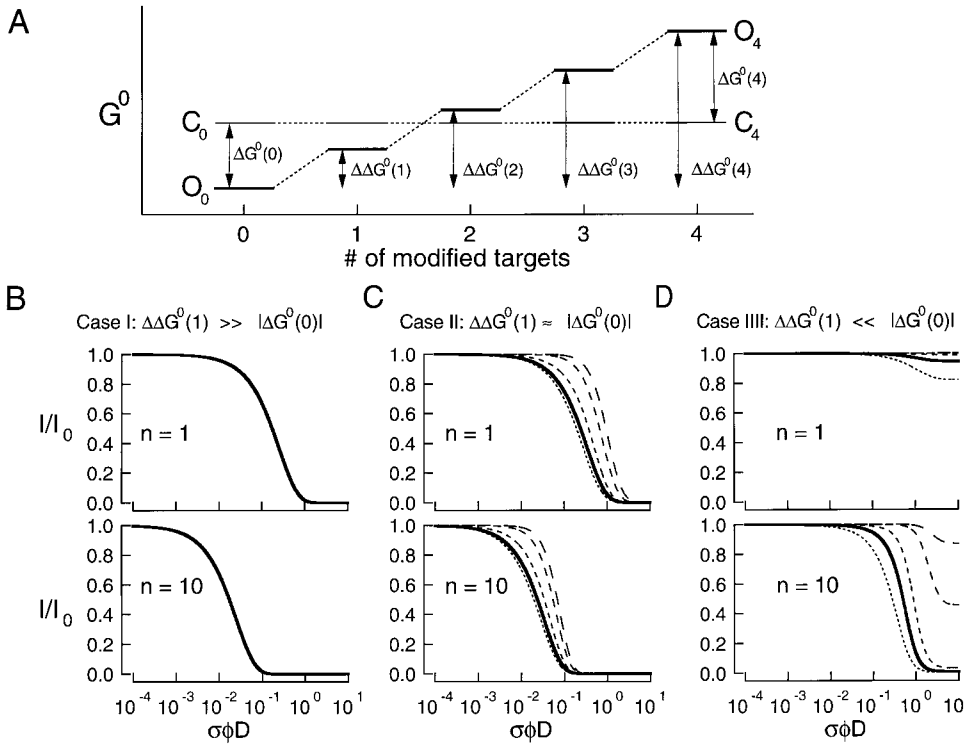

Figure 4. Energy additive model for channel current reduction by UV light. (A) Schematic showing the effect of modifying UV target residues on the standard free energy difference between open and closed channel states. The symbols O_k and C_k represent open and closed states of fully liganded channels with k modified target residues. $\Delta G^0(k)$ is the standard free energy difference between O_k and C_k, and $\Delta\Delta G^0(k)$ is the change in this free energy difference caused by modifying k targets. Since $\Delta\Delta G^0(k)$ is assumed to vary in linear proportion to k, the thermodynamic parameters are related as $\Delta G^0(k) = \Delta G^0(0) + k \cdot \Delta\Delta G^0(1)$. (B–D) UV dose–response relations calculated using energy additive model. Smooth curves were calculated using Eq. 6 for the following $\Delta G^0(0)$ values (*RT* units): −1.5 (dotted line), −3.0 (solid line), −4.6 (short-dashed line), −7.8 (medium-dashed line), and −9.9 (long-dashed line). These values correspond to the standard free energy differences for various channel/ligand combinations tested (Table II). $\Delta\Delta G^0(1)$ values were (*RT* units): (B) +40, (C) +4, and (D) +0.2. The top and bottom set of curves in each panel were calculated for the minimum (1) and maximum (10) possible number of tryptophan target residues per subunit.

2000). (b) Typical photochemical quantum yields for tryptophans in proteins are in the range $0.01 \leq \phi \leq 0.2$ (McLaren and Shugar, 1964; Vladimirov et al., 1970; Grossweiner, 1976). However, since ϕ depends on the protein environment around the target, these values should be considered only as a starting estimate. (c) Homo-oligomeric RET and OLF channels contain 10 tryptophan residues per subunit (Kaupp et al., 1989; Dhallan et al., 1990); thus, $1 \leq n \leq 10$. (d) The open probability of RET channels in saturating cGMP is ~0.95 (see Table II), corresponding to $\Delta G^0(0) = -3.0$ *RT* (see Eqs. 4 and 5). For OLF channels, $\Delta G^0(0) = -9.9$ *RT*. (e) As noted above, the observed decrease in P_o after irradiation implies that $\Delta\Delta G^0(1) > 0$. A narrower range of possible values for this parameter is obtained by considering the limiting value of $I(D)/I(0)$ for large values of *D*. If we denote this limit as *M*, then, from Eq. 6:

$$M = \lim_{D \to \infty} \frac{I(D)}{I(0)} = \frac{1 + \exp[\Delta G^0(0)]}{1 + \exp[\Delta G^0(0) + 4n \cdot \Delta\Delta G^0(1)]}. \quad (8)$$

Solving Eq. 8 for $\Delta\Delta G^0(1)$ yields:

$$\Delta\Delta G^0(1) = \frac{\ln\left\{\frac{(1-M) + \exp[\Delta G^0(0)]}{M \cdot \exp[\Delta G^0(0)]}\right\}}{4n}. \quad (9)$$

Using the estimate $M \leq 0.05$ (Middendorf et al., 2000, and Fig. 3 A) and the above values of *n* and $\Delta G^0(0)$ (Middendorf et al., 2000), evaluation of Eq. 9 yields $\Delta\Delta G^0(1) \geq +0.15$ *RT* for RET channels and $\Delta\Delta G^0(1) \geq +0.32$ *RT* for OLF channels.

The open probability of CNG channels can be varied by changing the channel sequence (e.g., RET vs. OLF channels; Goulding et al., 1994; Gordon and Zagotta, 1995b; Zong et al., 1998; Paoletti et al., 1999), by varying the identity of the activating ligand (e.g., cGMP vs. cAMP vs. no ligand; Goulding et al., 1994; Gordon and Zagotta, 1995b; Varnum et al., 1995), by introducing chemical species that bind to the channels (such as the transition metals Ni^{2+}, Zn^{+2}, and Co^{+2}; Ildefonse and Bennett, 1991; Ildefonse et al., 1993; Karpen et al., 1993; Gordon and Zagotta, 1995a), or by modifying them chemically; e.g., with *N*-ethyl maleimide (Finn et al., 1995; Gordon et al., 1997; Brown et al., 1998), copper phenanthroline (Gordon et al., 1997), or methanethiosulfonate reagents (Brown et al., 1998). By exploiting these factors, it is possible to vary $\Delta G^0(0)$ between −9.9 *RT* (OLF channels in saturating cGMP) and +11.9 RT (RET channels in the absence of ligand). Over this free energy range, the equilibrium constant for channel opening varies by nine orders of magnitude.

The next section presents theoretical UV dose–response relations calculated using the energy additive model. The curves predict how the UV dose–response

relation should vary for channels with different values of $\Delta G^0(0)$. The theory is then compared with the observed UV dose–response relations for CNG channels.

Effects of Varying $\Delta G^0(0)$ on the UV Dose–Response Relation in Saturating Ligand: Simulations

UV dose–response relations were calculated using Eq. 6, $\Delta G^0(0)$ values from Table II and values of n and $\Delta\Delta G^0(1)$, consistent with the constraints discussed in the previous section. When the simulated UV dose–response relations are plotted using a logarithmic abscissa, the quantum yield and absorption cross section of the targets affect only the absolute positions of the curves, not their shapes. We eliminated the curves' dependence on σ and ϕ by transforming the abscissa to the dimensionless coordinate $\sigma\cdot\phi\cdot D$ and comparing only the relative positions of the simulated curves on the dose axis.

The effect on the theoretical relations of varying $\Delta G^0(0)$ depended on the relative magnitudes of the free energy parameters $\Delta\Delta G^0(1)$ and $\Delta G^0(0)$, and on the number of target residues per subunit, n. Three limiting cases were examined.

Case I. If $\Delta\Delta G^0(1)$ is much larger than $|\Delta G^0(0)|$ (Fig. 4 B), then Eq. 6 reduces to Eq. 10:

$$\frac{I(D)}{I(0)} = f(0, D) = \exp(-4n\sigma\phi D). \qquad (10)$$

In this limit, the simulated UV dose–response relations were independent of $\Delta G^0(0)$ and the current approached an asymptote of zero for all possible target numbers. These predictions are consistent with the idea that photochemical modification of a single target residue abolishes the channel current, and that modification of additional targets has no measurable effect.

Case II. When $\Delta\Delta G^0(1)$ and $|\Delta G^0(0)|$ were comparable in magnitude (Fig. 4 C), decreasing $\Delta G^0(0)$ (i.e., making channel opening more favorable) shifted the simulated relations to the right along the abscissa and increased their slope. These trends reflect the larger number of target modifications (and the proportionately higher UV dose) that are needed to offset the increased initial relative stabilization of the channels' open state. Put another way, increasing the channels' initial open probability antagonizes the effect of UV.

Case III. If $\Delta\Delta G^0(1)$ was much smaller than $|\Delta G^0(0)|$ (Fig. 4 D), then increasing $-\Delta G^0(0)$ relative to $\Delta\Delta G^0(1)$ again shifted the simulated curves to the right along the abscissa and increased their slope, but also increased the limiting value of $I(D)/I(0)$. The latter effect occurs when the free energy cost of modifying all of the target residues, equal to $4n\cdot\Delta\Delta G^0(1)$, is not much larger than $|\Delta G^0(0)|$. In the limit that $4n\cdot\Delta\Delta G^0(1) << |\Delta G^0(0)|$, Eq. 6 reduces to Eq. 11:

$$\frac{I(D)}{I(0)} = \sum_{k=0}^{4n} f(k, D) = 1, \qquad (11)$$

and the UV effect on current amplitude disappears (Fig. 4 D, top).

For all three limiting cases, the curves for $n = 10$ were shifted to the left of those for $n = 1$ due to increased light collection by a larger number of targets. The slopes of the relations were sensitive to the number of target modifications needed to reduce the current significantly rather than the total number of target residues present in the channels.

Effects of Varying $\Delta G^0(0)$ on the UV Dose–Response Relation in Saturating Ligand: Experimental Results

This section compares the simulated curves of Fig. 4, B–D, to the observed UV dose–response relations for CNG channels with different initial free energy gaps. Varying the channels' amino acid sequence was the first of three methods used to alter $\Delta G^0(0)$. In saturating cGMP, channel opening is much less favorable for RET than for OLF channels [$\Delta G^0(0) = -3.0$ vs. -9.9 RT]. Results from several laboratories (Goulding et al., 1994; Gordon and Zagotta, 1995b; Gordon et al., 1997; Varnum and Zagotta, 1997) are consistent with the idea that this difference in gating efficacy results from a favorable interaction between an NH_2-terminal domain and the COOH-terminal cyclic nucleotide binding domain that occurs only in OLF channels (Varnum and Zagotta, 1997).

The UV dose–response relations for RET and OLF channels clustered into well-defined groups (Fig. 5 A), with the OLF channel cluster far to the right on the abscissa. The half-maximal dose, $D_{1/2}$, for each patch was estimated by fitting the experimental points with a smooth curve using Eq. 3. Each relation for patches expressing a given channel was then shifted along the abscissa so that $D_{1/2}$ for the shifted points was equal to the average $D_{1/2}$. Pooling the results in this way removed the variation in absolute UV sensitivity between patches and revealed the highly reproducible shapes of the UV dose–response relations for each channel type (Fig. 5 B). OLF channels were roughly four times less sensitive to UV than RET channels, and their UV dose–response relations were two and a half times steeper (Table I). For both channels, UV ultimately reduced the current to <5% of its initial value.

The open probability of CNG channels was also varied by adding low concentrations (~10 μM) of Ni^{2+} ions to the cytoplasmic surfaces of the patches. Ni^{2+} and other divalent transition metals potentiate the responses of CNG channels to cGMP (Ildefonse and Bennett, 1991; Ildefonse et al., 1993; Karpen et al., 1993) by binding to a histidine residue located between the S6 putative transmembrane segment and the consensus

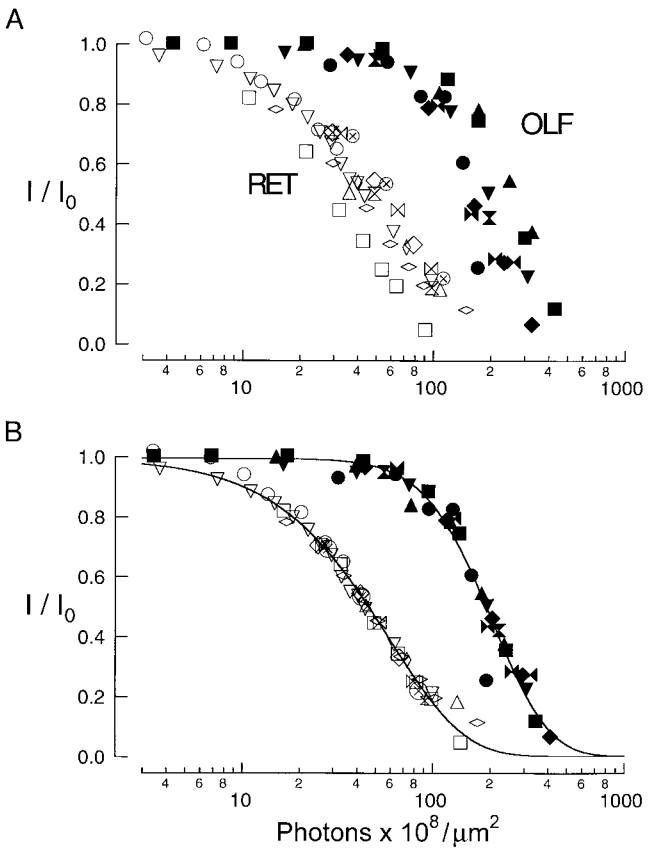

Figure 5. UV effects on currents through different CNG channels. (A) UV dose–response relations for RET and OLF channels activated by saturating (1 mM) cGMP. Fraction of current remaining is plotted as a function of the logarithm of the photon dose. Collected results from 10 experiments on RET channels (open symbols) and 7 experiments on OLF channels (solid symbols). Different symbols indicate separate experiments. (B) Same as in A, except results for each type of channel were shifted along the abscissa as in Fig. 3 A. Continuous curves are fits to the pooled results using Eq. 3 of the text. $D_{1/2}$ values and slope factors obtained from the fits are given in Table I. Patches were irradiated with 280 nm UV in the absence of cGMP.

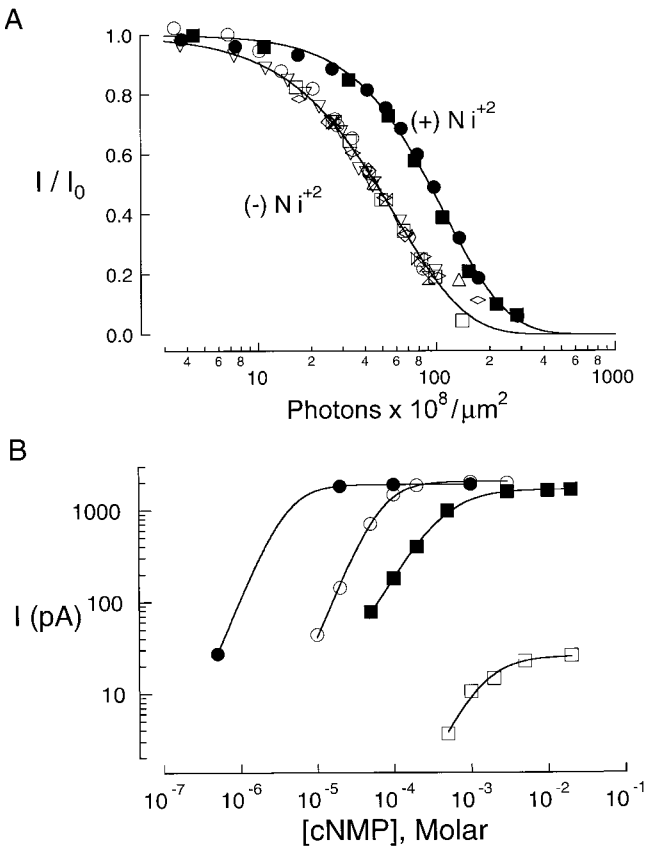

Figure 6. Effects of divalent nickel ions on the UV dose–response relation and the ligand dose–response relations of RET channels. (A) UV dose–response relations for channels activated by 1 mM cGMP in the presence (closed symbols, 3 experiments) or absence (open symbols, 10 experiments) of 10 μM cytoplasmic Ni^{2+}. Different symbols indicate separate experiments. Results were shifted along the abscissa as in Fig. 3 A. Continuous curves are fits to the combined results for cGMP or cGMP + Ni^{2+} using Eq. 3. $D_{1/2}$ values and slope factors from the fits are given in Table I. Channels were irradiated with 280 nm UV in the absence of cGMP. Since the washout of Ni^{2+} was extremely slow, it was present during irradiation when used. (B) Ligand dose–response relations of RET channels activated by cGMP (circles) and cAMP (squares) in the absence (open symbols) and presence (closed symbols) of 10 μM cytoplasmic Ni^{2+}. Patch current is plotted as a function of ligand concentration on double logarithmic coordinates. Continuous curves are fits to the results using the Hill equation (Eq. 1). The Hill coefficients (h), half-saturating ligand concentrations ($K_{1/2}$) and maximal currents [$I_{max}(0)$] obtained from the fits were: for cGMP + Ni^{2+}: h = 2.01, $K_{1/2}$ = 4.10 μM, and I_{max} = 1,902 pA; for cGMP, h = 2.01, $K_{1/2}$ = 69.9 μM, and I_{max} = 2,050 pA; for cAMP + Ni^{2+}, h = 1.58, $K_{1/2}$ = 398 μM, and I_{max} = 1,656 pA; for cAMP, h = 1.38, $K_{1/2}$ = 1,595 μM, and I_{max} = 27 pA. Results in B were recorded for one of the patches in A before irradiation, and agree with published results (Gordon and Zagotta, 1995a).

cGMP binding domain (Gordon and Zagotta, 1995a). Ni^{2+} may promote channel opening by binding more tightly to the open than to the closed state of the channel (Gordon and Zagotta, 1995a).

Adding Ni^{2+} ions reduced the UV sensitivity of RET channels activated by saturating cGMP (Fig. 6 A) approximately twofold, and increased the slope of the UV dose–response relation by ~70%. UV ultimately reduced the currents in the presence or absence of Ni^{2+} to <5% of their initial amplitudes. The effects of Ni^{2+} on the gating of the channels before irradiation (Fig. 6 B) agreed well with those reported previously (Gordon and Zagotta, 1995a): Ni^{2+} increased the channels' apparent affinities for cAMP and cGMP by factors of 4 and 15, respectively, and increased the current amplitude in saturating cAMP 60-fold.

The channels' gating energetics were also varied by changing the identity of the activating ligand. The current through RET channels activated by saturating cAMP is only ~2% of that activated by saturating cGMP (Kaupp et al., 1989; Goulding et al., 1992; Gordon and

Zagotta, 1995a; Varnum and Zagotta, 1996). This result, coupled with the finding that the unitary conductances of channels bound fully with cAMP and cGMP are the same (Sunderman and Zagotta, 1999), indicates that cAMP is a poorer agonist than cGMP. For OLF channels, the current amplitudes in saturating cAMP and cGMP are similar. The lower agonist potency of cAMP is manifested in this case as a decrease in the channels' apparent affinity for cAMP compared with cGMP (Goulding et al., 1994; Gordon and Zagotta, 1995b).

Fig. 7 shows UV dose–response relations for RET and OLF channels activated by saturating concentrations of cAMP and cGMP. Separate responses to cAMP and cGMP were measured for most of the patches after each UV dose. This approach eliminated variations in UV sensitivity between patches, enabling us to detect small differences in the UV dose–response relations of channels activated by each ligand. (10 μM Ni^{2+} was also included in the bath solutions for the experiments on RET channels. UV had an unusual effect on the currents through RET channels activated by cAMP in the absence of Ni^{2+} (see Fig. 14). Ni^{2+} was omitted in the experiments on OLF channels.)

For RET channels, substituting cGMP + Ni^{2+} for cAMP + Ni^{2+} increased $D_{1/2}$ by 72% and increased the slope factor of the relation by 70% (Fig. 7 A), basing the comparison on patches for which separate UV dose–response relations were obtained for both ligands. For OLF channels, substituting cGMP for cAMP increased $D_{1/2}$ by 42% and increased the slope factor of the relation approximately twofold (Fig. 7 B).

The results in Figs. 5–7 are summarized in Table I. Varying $\Delta G^0(0)$ by the three types of energetic perturbations had similar effects on the channels' UV dose–response relations. Making $\Delta G^0(0)$ more negative shifted the UV dose–response relations to the right on the abscissa and increased their slopes. This correlation between shift and slope is explained by the energy additive model. As $\Delta G^0(0)$ is made more negative, more targets must be modified to invert the relative free energies of the channels' open and closed states and lower P_o. The steepness of the UV dose–response relation increases in proportion to the number of required modifications. It takes a larger photon dose to modify more targets, leading to the parallel increase in $D_{1/2}$.

The observed effects of varying $\Delta G^0(0)$ on the UV dose–response relations (Figs. 5–7) are consistent with Case II (Fig. 4 C), but not Case I (Fig. 4 B) or Case III (Fig. 4 D) of the energy additive model. We conclude that (a) UV reduced the currents in saturating cGMP by lowering the channels' open probability, and (b) $\Delta\Delta G^0(1)$ is comparable in magnitude to $|\Delta G^0(0)|$ for RET and OLF channels.

Figs. 5–7 show only 4 of 10 possible pairwise comparisons between the UV dose–response relations for the five channel/ligand/Ni^{2+} combinations studied. 8 of 10 pairs (including those in Figs. 5–7) exhibited the positive correlation between $-\Delta G^0(0)$ and $D_{1/2}$ that is predicted by Case II of the energy additive model. Two pairs violated the expected trend. First, the half-maximal UV dose was slightly larger for RET channels acti-

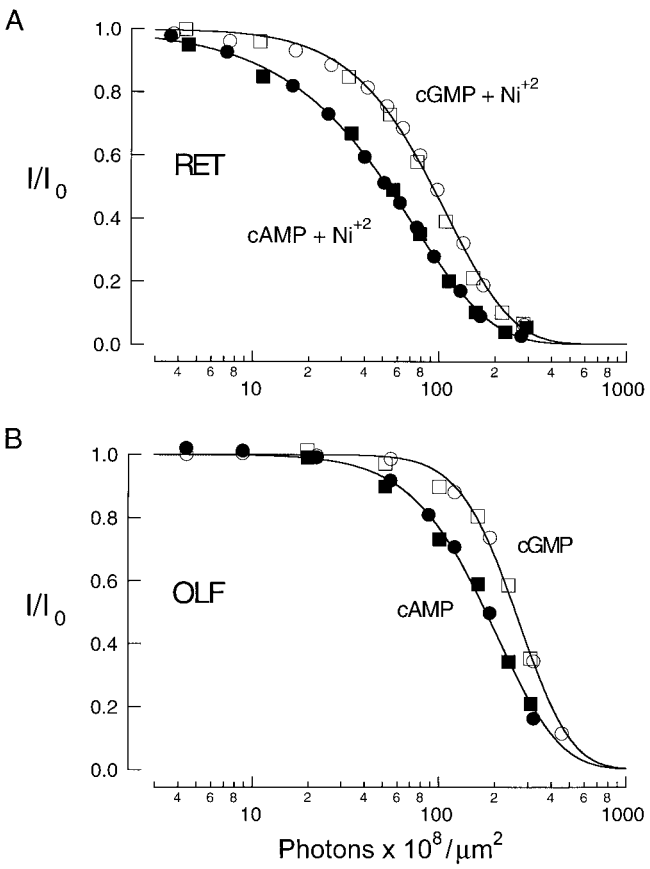

Figure 7. UV effects on currents through CNG channels activated by different cyclic nucleotide ligands. (A) UV dose–response relations for RET channels activated by cAMP and cGMP. Results are from two patches. For both experiments, the patch current in saturating cAMP and in saturating cGMP solutions was measured after each UV exposure. Closed symbols are for cAMP, open symbols are for cGMP. Ligand concentrations were, for patch 1 (circles): cAMP, 3 mM, and cGMP, 1 mM; for patch 2 (squares): cAMP, 10 mM, and cGMP, 1 mM. Continuous curves show fits to the combined results for cAMP or cGMP using Eq. 3. The $D_{1/2}$ and slope factors from the fits are given in Table I. Pre-UV current amplitudes were: for patch 1, I_{cAMP} = 1,603 pA and I_{cGMP} = 1,926 pA; for patch 2, I_{cAMP} = 3,311 pA and I_{cGMP} = 4,251 pA. Bath solutions for all experiments in A contained 10 μM Ni^{2+} (see text). (B) UV dose–response relations for OLF channels activated by saturating (2 mM) cAMP or saturating (1 mM) cGMP. Results are from two patches. For each patch, currents were recorded before UV and after each UV dose in both cGMP and cAMP. Other experimental conditions were as in A, except Ni^{2+} was omitted from the bath solutions. Smooth curves are fits as in A. $D_{1/2}$ and slope factors from the fits are given in Table I. Pre-UV current amplitudes were: for patch 1 (circles), I_{cAMP} = 4,652 pA and I_{cGMP} = 4,742 pA; for patch 2 (squares), I_{cAMP} = 359 pA and I_{cGMP} = 365 pA. Patches in A and B were irradiated with 280 nm UV in the absence of cyclic nucleotides.

vated by cAMP + Ni^{2+} than by cGMP alone, even though $-\Delta G^0(0)$ is only about half as large (Fig. 8 A and Table II). A more significant deviation from the expected trend is shown in Fig. 8 B. The fit to the UV dose–response relation for RET channels activated by saturating cGMP + Ni^{2+} from A (reproduced as a dashed line in Fig. 8 B) is shifted leftward on the abscissa from the relation for OLF channels activated by cAMP, even though $-\Delta G^0(0)$ is much larger (Table II).

The energy additive model also predicts a positive correlation between $-\Delta G^0(0)$ and the slope factor for a channel's UV dose–response relation. 9 of 10 channel/ligand/Ni^{2+} combinations followed this prediction. The lone discrepancy again occurred for the second of two pairs described above: the slope factor was smaller for RET/cGMP/Ni^{2+} compared with OLF/cAMP, despite its larger initial free energy gap.

Fig. 8, C and D, shows explicitly the relations between the UV and thermodynamic parameters for all of the channel/ligand combinations studied. When plotted as a function of $-\Delta G^0(0)$ (Fig. 8 C), the $D_{1/2}$ values clustered into two groups, with the points for OLF channels displaced above those for RET channels. Assuming that $D_{1/2}$ for each channel type at any intermediate value of $-\Delta G^0(0)$ may be obtained by interpolating between measured values, the results suggest that OLF channels have a lower UV sensitivity than RET channels with the same value of $-\Delta G^0(0)$. The slope factors of the UV dose–response relations for OLF channels were also larger than those for RET channels after correcting for differences in $\Delta G^0(0)$ (Fig. 8 D).

What factors are responsible for the differences between the UV dose–response relations of RET and OLF channels with the same value of $\Delta G^0(0)$ (Fig. 8, C and D)? A difference in the number or quantum yields of the UV targets in the two types of channels could account for the observed variation in $D_{1/2}$ (Fig. 8 C), but is not expected to cause a difference in the slopes of the channels' UV dose–response relations, as was observed (Fig. 8 D). The results in Fig. 8 D are more consistent with the idea that the free energy cost of target modification is different in RET and OLF channels. To test this hypothesis, we fit the results in Figs. 5–7 simultaneously, using the energy additive model (Eq. 6). As predicted, the $\Delta\Delta G^0(1)$ values obtained from the fits were different for RET and OLF channels. In addition, the free energy costs varied for a given channel activated by different ligands. The smooth curves in Fig. 9, A and B, show the fits for $n = 2$; excellent fits were obtained for all target numbers greater than one per subunit. The magnitude of $\Delta\Delta G^0(1)$ for each channel/ligand combination (Fig. 9 C) was relatively independent of the number of targets for $n \geq 2$, probably because the total free energy cost of modifying two targets per subunit was sufficient to reduce the open probability close to zero. Additional targets, if present, are essentially undetectable because of the negligible incremental effect of their modification on the current amplitude.

The differences in $\Delta\Delta G^0(1)$ for RET and OLF channels activated by a given ligand are not surprising. Some of the tryptophan residues occupy inequivalent positions in RET and OLF channels. The associated $\Delta\Delta G^0(1)$ values would almost certainly differ if any of these tryptophans were UV targets. Furthermore, the $\Delta\Delta G^0(1)$'s might differ even for homologous target residues in the two channels, since the free energy change associated with mutating equivalent residues in related proteins often depends on the environment of the mutated residue (Creighton, 1993).

The differences in $\Delta\Delta G^0(1)$ for the same channel activated by different ligands implies that at least one of the target residues interacts with the cyclic nucleotides, their binding site, or with structures that affect the coupling between ligand binding and channel opening.

The estimated photochemical quantum yields varied inversely with the number of targets per subunit, from ~2% for $n = 1$ to 0.2% for $n = 10$ (Fig. 9 D). The reciprocal relationship between n and ϕ is expected due to their appearance as a product in the exponent in Eq. 7.

UV Sensitivity of Pore Tryptophan Mutants

In the preceding paper (Middendorf et al., 2000), we described an attempt to identify the target tryptophan residue(s) in RET channels by measuring the UV sensitivities of mutant CNG channels in which 1 of the 10 native tryptophans per subunit was replaced by another amino acid. We expected such mutations to decrease or possibly eliminate the channels' UV sensitivity if the replaced residues were UV targets. To our surprise, the mutant W353Y, which substitutes tyrosine for a highly conserved tryptophan residue in the channel pore, was seven times more UV sensitive than the parent RET channel.

A possible explanation for this result is that the W353Y mutation disrupts channel opening. The energy additive model (Fig. 4 A) predicts that, other factors being equal, a mutation that destabilizes the channels' open state relative to the closed state should decrease the number of target modifications that are needed to reduce the open probability to a small value. Other characteristics of RET/W353Y channels were consistent with this hypothesis. The apparent expression of the mutant channels was poor; cGMP-dependent currents were small and were detected infrequently, and then only in the presence of low concentrations of cytoplasmic Ni^{2+}. Since Ni^{2+} ions promote channel opening (Gordon and Zagotta, 1995a) without affecting the conductance of open channels (Sunderman and Zagotta, 1999), it is likely that the open probability of RET/W353Y channels is very low in the absence of Ni^{2+}.

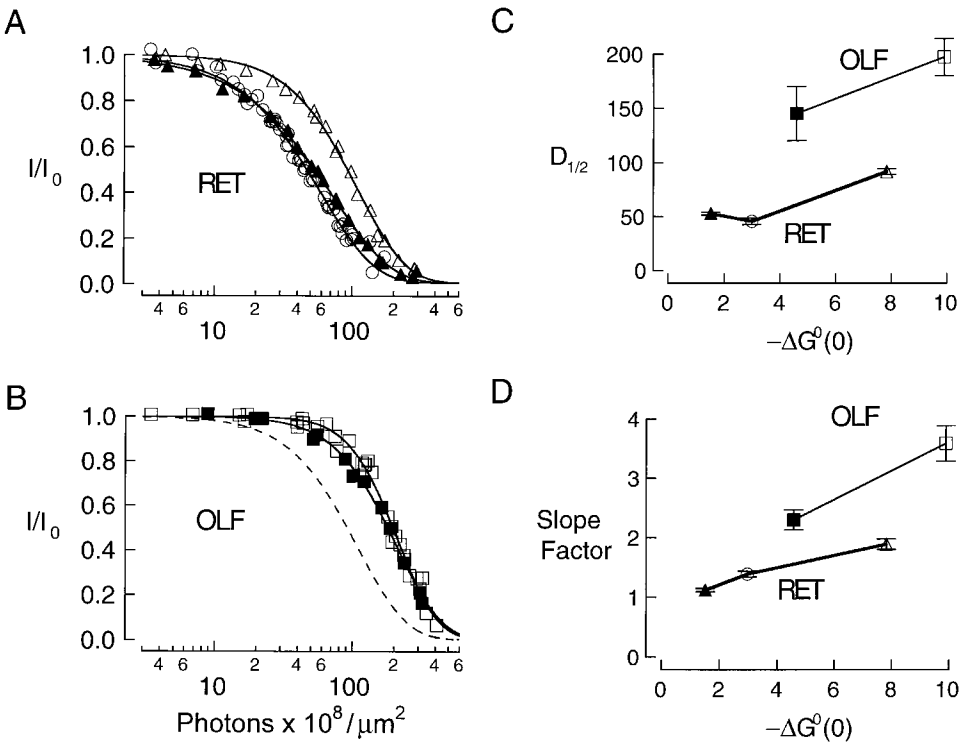

Figure 8. Evidence for differential effects of UV light on RET and OLF channels. (A) UV dose–response relations for RET channels activated by: saturating (1 mM) cGMP (○, results from Fig. 5); 1 mM cGMP + 10 μM Ni^{2+} (△, results from Fig. 6 A); and saturating (3 or 10 mM) cAMP + 10 μM Ni^{2+} (▲, results from Fig. 7 A). (B) UV dose–response relations for OLF channels activated by: saturating (1 mM) cGMP (□, results from Fig. 5); and saturating (2 mM) cAMP (■, results from Fig. 7 B). The smooth curves in A and B are fits to the combined results for each channel/ligand combination using Eq. 3 of the text. The $D_{1/2}$ values and the slope factors obtained from the fits are listed in Table I. The dashed curve is a reproduction of the fit in A to the results for RET channels activated by saturating cGMP+ Ni^{2+} (△). (C) $D_{1/2}$ values (in photons $\times 10^8 \cdot \mu m^{-2}$) obtained from the fits to the UV dose–response relations in A and B, plotted as a function of the initial free energy difference between open and closed channel states, $\Delta G^0(0)$ (see Table II). (D) Slope factors obtained from the fits in A and B, plotted as a function of $\Delta G^0(0)$. Symbols in C and D correspond to the same channel/ligand pairs in A and B.

Due to the difficulty in obtaining cyclic nucleotide–dependent currents from RET/W353Y channels, we did not characterize this mutant further. Instead, we prepared the equivalent mutant in the OLF channel background, OLF/W332Y. Assuming that the energetic effect of the mutation is similar in the two backgrounds, we reasoned that the open probability in saturating cGMP may be much higher for OLF/W332Y compared with RET/W353Y channels because the allosteric opening transition is much more energetically favorable for wild-type OLF compared with wild-type RET channels (Goulding et al., 1994; Gordon and Zagotta, 1995b; Gordon et al., 1997; Varnum and Zagotta, 1997). Consistent with this prediction, large (many nanoampere) currents were detected in oocytes injected with cRNA coding for OLF/W332Y channels. OLF/W332Y channels activated by saturating (1 mM) cGMP were about six times more UV sensitive than the parent OLF channels (Fig. 10 A). The UV dose–response relation of OLF/W332Y channels was also 2.5× shallower than that of wild-type OLF channels. Similar results were obtained for a second OLF channel mutant in which histidine replaced tryptophan 332 (Fig. 10 B). These results are consistent with the hypothesis that replacing the conserved pore tryptophan residue with tyrosine or histidine lowers the channels' open probability. Two additional lines of evidence support this idea. First, the half-saturating cGMP concentration before UV was greater for OLF/W332Y channels ($K_{1/2}$ = 17.7 μM) than for wild-type OLF channels ($K_{1/2}$ = 2.5 μM, Fig. 10 C). In potassium channels, which have a similar pore sequence to CNG channels, the tryptophan residue equivalent to W332 is located near the extracellular side of the channel pore (Doyle et al., 1998). If W332 occupies a similar position in OLF channels, it is probably located far from the cytoplasmic COOH-terminal cyclic nucleotide–binding domain. Thus, it is more likely that the effect of the mutation is to disrupt the allosteric channel opening transition, rather than to alter the cGMP binding step. The ratio of the current amplitudes in saturating cAMP and saturating cGMP (Fig. 10 D) was also smaller for OLF/W332Y and OLF/W332H channels than for wild-type OLF channels, providing direct evidence that the pore mutations lowered the channels' open probability.

Since UV light may modify tyrosine residues in proteins (McLaren and Shugar, 1964), it was possible that replacing tryptophan 332 with tyrosine in the OLF channel increased the UV sensitivity because tyrosine at position 332 is a "better" target than the original tryptophan. In this context, "better" means that the target is modified more readily and/or that its modification has a higher free energy cost. This hypothesis was easily tested: if photochemical modification of tyrosine 332 dominated the UV effect on OLF/W332Y channels, the

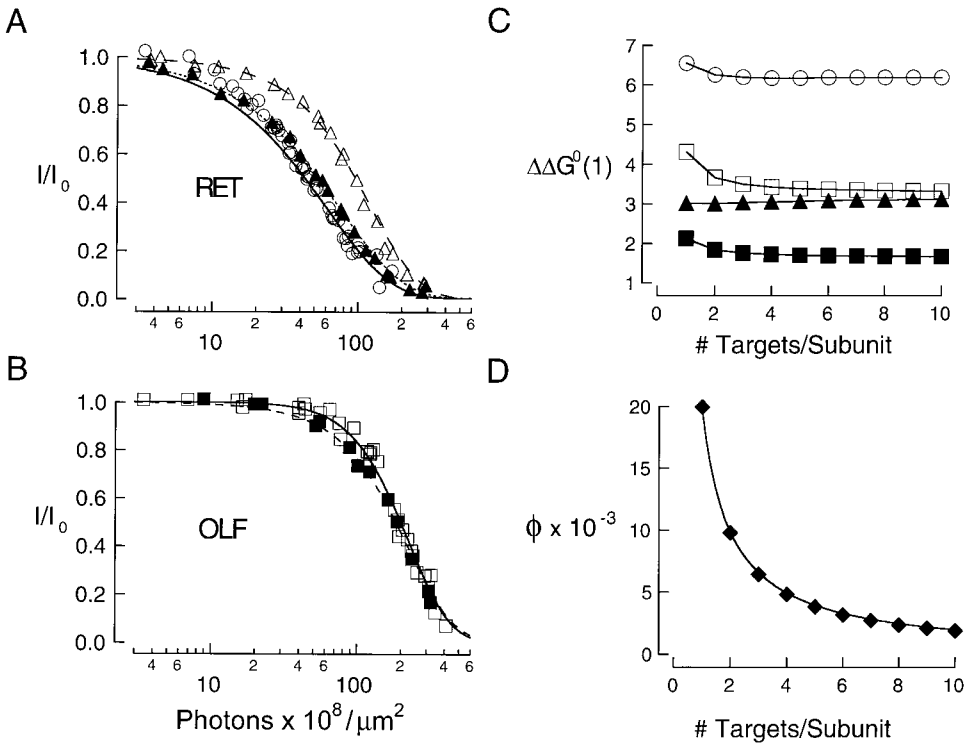

Figure 9. Modeling of UV effect on CNG channel currents. (A and B) UV dose–response relations for: (A) RET and (B) OLF channels. Results are the same as in Fig. 8, A and B. Relations were fit using the energy additive model (Eq. 6) for all possible values of n, the number of UV target residues per channel subunit. The continuous curves show fits for $n = 2$; excellent fits (not shown) were also obtained for $3 \leq n \leq 10$. The free energy cost of target modification, $\Delta\Delta G^0(1)$, was allowed to vary for the different channel/ligand pairs. The photochemical quantum yield, ϕ, was constrained to be the same for RET and OLF channels for all conditions studied. $\Delta G^0(0)$ values used in the fits are given in Table II. (C) Free energy cost for target modification in CNG channels. $\Delta\Delta G^0(1)$ values obtained from the fits in A and B are plotted as a function of n. The solid lines connect the points. The average values of $\Delta\Delta G^0(1)$ for $2 \leq n \leq 10$ (RT units) were: for RET/cGMP (○), 6.19 ± 0.03; for OLF/cGMP (□), 3.41 ± 0.11; for RET/cAMP (▲), 3.07 ± 0.04; and for OLF/cAMP (■), 1.72 ± 0.05. (D) Quantum yield for target modification in CNG channels. Quantum yields (◆), obtained from the fits in A and B are plotted as a function of n. The smooth curve is a fit to the results using the relation $\phi = B/n$, with the constant $B = 0.02$.

wavelength dependence of the mutant channels' UV sensitivity should match the wavelength dependence of tyrosine absorption. The UV sensitivity of OLF/W332Y channels was measured at two wavelengths for which the relative absorption probabilities of tryptophan and tyrosine are very different. Increasing the excitation wavelength from 280 to 300 nm increased $D_{1/2}$ by a large factor (Fig. 11 A). However, the slopes of the mutant channels' UV dose–response relations were the same at 280 and 300 nm, indicating that the UV wavelength affected the probability of target modification, but not the nature of the modification or the mechanism of the current reduction. This result is a necessary precondition for identifying the target residues from the wavelength dependence of the UV sensitivity.

The ratio of the UV sensitivities of OLF/W332Y channels at 280 and 300 nm (15.9 ± 6.3, Fig. 11 C) was similar to the corresponding ratio of 15.7 for tryptophan absorption in aqueous solution, but was much smaller than the ratio of 111 for tyrosine absorption at these wavelengths. This comparison indicates that the photochemical reaction(s) that reduces the current amplitude in the mutant channels is initiated by absorption in one or more of the remaining tryptophan residues, with little or no contribution from the newly introduced tyrosine residue at position 332. The wavelength dependence of the UV sensitivity of OLF/W332H channels was also consistent with tryptophan absorption (Fig. 11, B and C).

Consistent with the lower agonist efficacy of cAMP (Fig. 10 D), OLF/W332Y channels were more sensitive to UV when activated by saturating cAMP than when activated by saturating cGMP (Fig. 12 A). Similar results were obtained for OLF/W332H channels activated by these two ligands (Fig. 12 B). Although the differences in $D_{1/2}$ and slope for the channels activated by the two ligands were not large when averaged across all experiments, separate responses to cAMP and cGMP were recorded after each UV dose for most of the patches. The UV dose–response relations in cAMP were always left-shifted and shallower than the relations in cGMP.

Mechanism of Current Increase by UV

UV increased the current through CNG channels activated by low concentrations of cGMP (Figs. 1 B and 2 B). In the following sections, we consider the mechanism of this second effect of UV. We ask: (a) by what mechanism does UV increase the currents? and (b) why does UV increase the current at low concentrations of ligand but decrease the current at higher concentrations of ligand?

The magnitude of the current increase by UV de-

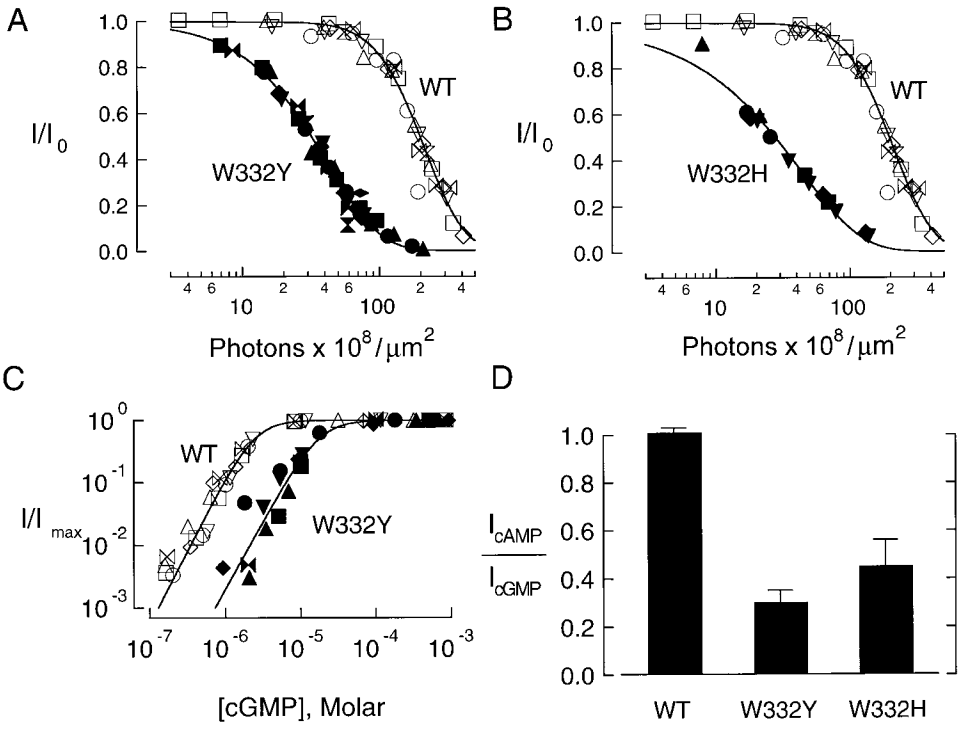

Figure 10. UV sensitivity and gating properties of CNG channels lacking a conserved pore tryptophan residue. (A and B) UV dose–response relations in saturating (1 mM) cGMP for OLF channels (open symbols, A and B, seven experiments), OLF/W332Y mutant channels (solid symbols, A, eight experiments), and OLF/W332H mutant channels (solid symbols, B, five experiments). Results from experiments on each type of channel were shifted along the abscissa as in Fig. 3 A. Different symbols represent separate experiments. Continuous curves are fits to the pooled results for each construct using Eq. 3. $D_{1/2}$ values and slope factors from the fits are given in Table I. Patches were irradiated with 280 nm UV in the absence of cGMP. (C) Cyclic GMP dose–response relations for OLF channels (open symbols, six experiments) and OLF/W332Y mutant channels (solid symbols, six experiments) before irradiation. The cGMP-activated current, I, divided by the maximal current in 1 mM cGMP, I_{max}, is plotted as a function of cGMP concentration on double logarithmic axes. Results from each experiment were shifted along the abscissa so that the half-saturating ligand concentration, $K_{1/2}$, was equal to the average value of $K_{1/2}$ for all experiments on the same channel. Different symbols represent separate experiments. Continuous curves are fits to the pooled results for each type of channel using the Hill equation (Eq. 1). The fitting parameters were: for OLF channels, $h = 2.35$ and $K_{1/2} = 2.47$ μM; for OLF/W332Y channels, $h = 2.17$ and $K_{1/2} = 17.7$ μM. (D) Relative efficacies of cAMP and cGMP for activating wild-type OLF, OLF/W332Y mutant, and OLF/W332H mutant channels. Ordinate is the ratio of the current amplitude in saturating cAMP (>3 mM) to that in saturating cGMP (1 mM). The current ratios, (mean ± SEM) and the number of experiments (in parentheses) were: for OLF, 1.01 ± 0.02 (4); for OLF/W332Y, 0.30 ± 0.05 (8); and for OLF/W332H, 0.45 ± 0.11 (5).

pended on the cGMP concentration (Figs. 1 C and 2 C). This result is not expected if UV increased the conductance of a single open state of the channels or enhanced their cGMP binding affinity, since either effect should alter the current by a constant fraction at all ligand concentrations. However, RET channels have multiple open states with different unitary conductances, and the relative occupancy of these levels depends on the cyclic nucleotide concentration (Ildefonse and Bennett, 1991; Taylor and Baylor, 1995; Ruiz and Karpen, 1997; Ruiz and Karpen, 1999). Thus, we cannot rule out the possibility that UV alters the channels' ligand dose–response relation by exerting differential UV effects on the unitary conductances of the various open states. The latter hypothesis is difficult to test because UV-activated conductances in the oocyte membrane preclude analysis by single channel recording (Middendorf et al., 2000). Instead, we investigated the effect at the macroscopic level by asking whether the observed current increase is consistent with UV effects on the channels' open probability or their unitary conductance.

Since the opposing UV effects on channel current were observed in some cases within the same patch (Figs. 1 C and 2 C), it is likely that the channels contain at least two distinct types of target residues. If both UV effects are on the channels' open probability, then modification of the two types of targets must exert opposite effects on the channels' gating energetics. For simplicity, we identify the two types of targets by the symbols (+) and (−), which refer to the sign of the free energy change associated with their modification. As noted earlier, the positive free energy cost associated with modification of a (+) target, $\Delta\Delta G^0(1+)$, has the effect of decreasing P_o (Fig. 4 A). The quantity $\Delta\Delta G^0(1-)$ is negative, consistent with the idea that modification of (−) targets stabilizes the channels' open state(s) relative to their closed state(s), and thereby increases P_o (Fig. 13 A). For simplicity, it is assumed in Fig. 13 A that the entire effect of modifying the (−) targets is on the free energy of the channels' open state.

We used the energy additive model to test the idea that UV increased the currents by enhancing the channels'

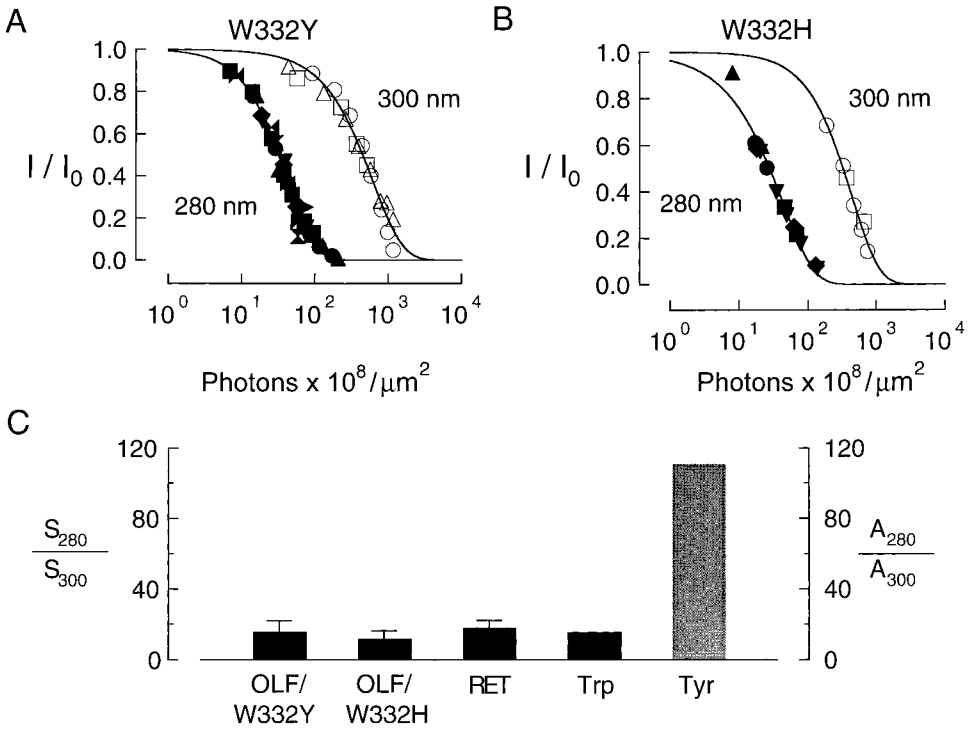

Figure 11. Wavelength dependence of the UV effect on mutant CNG channels lacking a conserved pore tryptophan residue. (A and B) UV dose–response relations in saturating (1 mM) cGMP for (A) OLF/W332Y and (B) OLF/W332H mutant channels irradiated with 280 nm UV (solid symbols) or 300 nm UV (open symbols). Collected results from eight experiments at 280 nm and three experiments at 300 nm for OLF/W332Y, and five experiments at 280 nm and three experiments at 300 nm for OLF/W332H. Results were shifted along the abscissa as in Fig. 3 A. Different symbols represent separate experiments. Continuous curves are fits to the pooled results using Eq. 3. $D_{1/2}$ values and slope factors from the fits are given in Table I. Patches were irradiated in the absence of cGMP. (C) Wavelength dependence of photon absorption by tryptophan and tyrosine compared with wavelength dependence of CNG channel UV sensitivity. The left-hand ordinate, S_{280}/S_{300}, is the ratio of the channels' UV sensitivities at 280 and 300 nm (defined as the reciprocals of the corresponding $D_{1/2}$ values). The UV sensitivity ratios were 15.9 ± 6.3 (mean ± SEM) for OLF/W332Y channels and 11.9 ± 4.5 for OLF/W332H channels. The UV sensitivity ratio of 17.1 ± 2.0 for wild-type RET channels (Middendorf et al., 2000) is shown also for comparison. The right-hand ordinate, A_{280}/A_{300}, is the ratio of the photon absorption probabilities in aqueous solution at 280 and 300 nm. The absorption probability ratios were 15.7 for tryptophan and 111 for tyrosine, and were computed from their absorption spectra using Eq. 15 of Middendorf et al. (2000).

open probability. Theoretical UV dose–response relations were calculated for channels with different $\Delta G^0(0)$ values using Eq. 6 with $\Delta\Delta G^0(1) < 0$, and then compared with the observed relations for channels with a range of different, but very low, initial open probabilities.

Effect of Varying $\Delta G^0(0)$ on the Current Increase by UV: Simulations

The calculated UV dose–response relations were characterized by fitting with a modified version of the all-or-none model (Middendorf et al., 2000). The fits provided quantitative estimates for the curves' horizontal positions, maximal slopes, and maximum fractional current increases. The model assumes that each channel subunit contains n independent and identical (−) targets and no (+) targets, and that UV has no effect on the channel current until modification of a critical number of the targets (denoted n^*) increases the current by a factor M. These ideas are described by the relation:

$$i_{sc}(k)P_o(k) = \begin{cases} i_{sc}(0)P_o(0);\ k < n^* \\ Mi_{sc}(0)P_o(0);\ k \geq n^* \end{cases}, \qquad (12)$$

where the index k denotes the number of modified (−) targets. Because UV can increase P_o to a value no greater than unity, the maximum fractional current increase is equal to $1/P_o(0)$. Eq. 12 ignores the effect of modifying the (+) targets, which will be incorporated at a later stage.

The UV dose–response relation for the modified all-or-none model is obtained by combining Eq. 12 of this paper with Eq. 25 of the preceding paper (Middendorf et al., 2000), yielding:

$$\frac{I(D)}{I(0)} = 1 - (1 - M)[1 - \exp(-\sigma\phi D)]^{n^*}. \qquad (13)$$

In Eq. 13, σ and ϕ are the absorption cross section and quantum yield of a (−) target, respectively, and D is the photon dose. The slope factor n^* provides a measure of the steepness of the relation.

As before (Figs. 4, B–D), the effect of varying $\Delta G^0(0)$ on the simulated UV dose–response relations depended on the relative magnitudes of the free energy parameters $\Delta\Delta G^0(1-)$ and $\Delta G^0(0)$. Three limiting cases were considered.

Case IV: in the limit that $-\Delta\Delta G^0(1-)$ is much larger than $|\Delta G^0(0)|$ (Fig. 13 B), Eq. 6 reduces to:

$$\frac{I(D)}{I(0)} = [1 - f(0, D)] \cdot \{1 + \exp[\Delta G^0(0)]\}. \qquad (14)$$

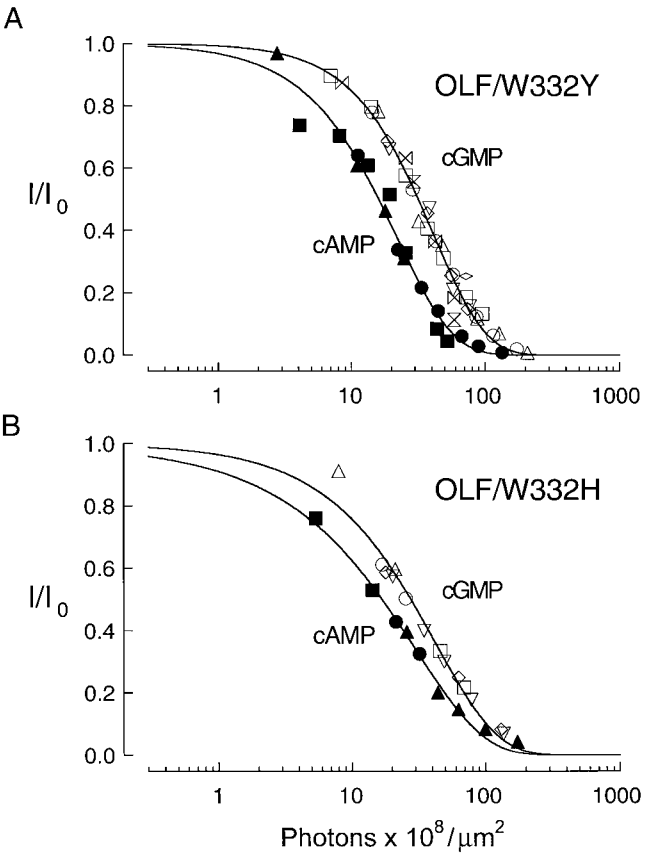

Figure 12. UV effects on currents through CNG channel pore tryptophan mutants activated by different ligands. (A and B) UV dose–response relations for OLF/W332Y (A) and OLF/W332H (B) mutant channels activated by saturating cAMP (1 mM, solid symbols) or saturating cGMP (1 mM, open symbols). Collected results from three experiments in cAMP and eight experiments in cGMP for OLF/W332Y channels, and three experiments in cAMP and five experiments in cGMP for OLF/W332H channels. Different symbols represent separate experiments. Results from separate experiments on each channel/ligand pair were combined as described in Fig. 3 A. Continuous curves are fits to the combined results for each channel activated by cGMP or cAMP using Eq. 3. $D_{1/2}$ values and slope factors from the fits are given in Table I. Channels were irradiated with 280 nm UV in the absence of ligand.

Using Eqs. 4 and 5, Eq. 14 simplifies further to Eq. 15:

$$\frac{I(D)}{I(0)} = \frac{1 - f(0, D)}{P_o(0)}, \qquad (15)$$

where $P_o(0)$ denotes the channels' open probability before irradiation. In this limit, the fractional current increase after UV reached the maximum possible value of $M = 1/P_o(0)$, regardless of the number of UV targets in the channels. On the other hand, the positions of the relations on the abscissa and their slopes were not affected by varying $\Delta G^0(0)$. These effects are consistent with the idea that modification of a single (−) target increases the channels' open probability to a value near unity if the free energy cost of target modification is both negative and much larger in absolute magnitude than $\Delta G^0(0)$. Due to the reciprocal relation between M and $P_o(0)$, the maximum fractional current increase may be quite large for low values of $P_o(0)$ (note the logarithmic ordinate in Fig. 13 B), but is negligible for $P_o(0) \approx 1$.

Case V: if $-\Delta\Delta G^0(1-)$ was comparable to $|\Delta G^0(0)|$ (Fig. 13 C), the fractional current increase after UV again depended on $\Delta G^0(0)$. For $n = 1$, the magnitude of the current enhancement by UV increased as $\Delta G^0(0)$ was made more positive, but did not reach the maximum possible value of $1/P_o(0)$. For $\Delta G^0(0) = +7.0$ (corresponding to OLF channels in the absence of ligand), $I(D)/I(0)$ reached only 5% of the maximum possible value, but, for $\Delta G^0(0) = +3.91$ (corresponding to RET channels activated by saturating cAMP), the current increased to nearly half the maximum possible value. For a large number of targets, the fractional current increase did approach a value of $1/P_o(0)$. The relations also shifted to the right along the abscissa and became steeper as $P_o(0)$ was decreased [i.e., as $\Delta G^0(0)$ was made more positive], but these effects were modest compared with those on the current amplitude.

Case VI: in the limit that $-\Delta\Delta G^0(1)$ was much smaller than $|\Delta G^0(0)|$ (Fig. 13 D), the simulated curves again shifted to the right along the abscissa and became steeper as $\Delta G^0(0)$ was increased. However, the current asymptotes in this limit were much smaller than $1/P_o(0)$, regardless of the number of targets. This latter effect occurred when the total free energy change associated with modifying all of the target residues (equal to $4n \cdot \Delta\Delta G^0(1)$, was insufficient to offset a large, positive value of $\Delta G^0(0)$. In the limit that $-4n \cdot \Delta\Delta G^0(1) << |\Delta G^0(0)|$, Eq. 6 reduces to Eq. 16:

$$\frac{I(D)}{I(0)} = \sum_{k=0}^{4n} f(k, D) = 1, \qquad (16)$$

and the UV effect on the current amplitude disappears (Fig. 13 D, top). With these predictions in hand, we turn to experimental measurements of UV dose–response relations for two channel/ligand combinations with low open probabilities: (a) RET channels activated by saturating concentrations of the poor agonist cAMP, and (b) OLF channels in the absence of ligand.

Effect of Varying $\Delta G^0(0)$ on the Current Increase by UV: Experimental Results

The open probability of RET channels activated by saturating cAMP is only ~1.5% (Goulding et al., 1994; Varnum and Zagotta, 1996). UV increased the currents through RET channels activated by saturating (20 mM) cAMP approximately threefold (Fig. 14 A). Similar results (not shown) were obtained for channels activated by 5 mM cAMP. The same UV dose decreased the cur-

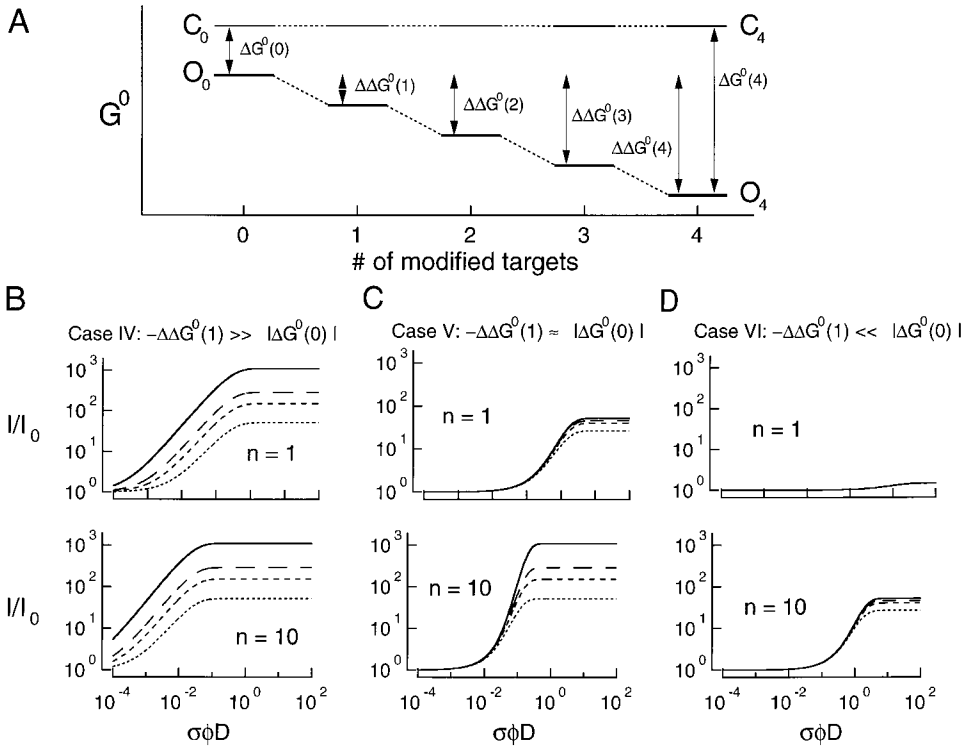

Figure 13. Energy additive model for increase in channel open probability by UV light. (A) Schematic showing effect of modifying (−) targets (see text) on the standard free energy difference between the channels' open and closed states. Symbols are equivalent to those in Fig. 4. (B–D) UV dose–response relations calculated using energy additive model. Smooth curves were calculated using Eq. 6 for the following $\Delta G^0(0)$ values (RT units): +7.0 (solid line), +5.7 (long-dashed line), +5.0 (medium-dashed line), and +3.9 (short-dashed line). $\Delta\Delta G^0(1)$ values (RT units) were: (B) −40; (C) −1; and (D) −0.1. The top and bottom set of curves in each panel were calculated for 1 and 10 (−) target residues per channel subunit, respectively.

rent elicited by saturating (1 mM) cGMP nearly fivefold for this same patch (Fig. 14 B). The UV dose–response relations for this patch are shown in Fig. 14, C (cAMP) and D (cGMP). Note the 100-fold difference in vertical scales in Fig. 14, C and D. The current increase in cAMP reached a maximum after a dose of 5×10^9 photons $\cdot$ μm^{-2}. Fitting the UV dose–response relation in cAMP with the modified all-or-none model (Eq. 13) yielded estimates of 7.7×10^9 photons $\cdot$ μm^{-2} for $D_{1/2}$, 0.85 for the slope factor, and 5.7 for the maximum fractional current increase. The value of M was only about one fifth of the maximum possible value [$1/P_o(0) = 27$]. The $D_{1/2}$ and slope factors for the UV dose–response relation in saturating cGMP were similar to those obtained for other RET channel patches (Table I). The opposing effects of UV on RET channel currents activated by saturating concentrations of the two ligands suggest that the channels' initial open probability, rather than the absolute number of bound ligands, determined the sign of the change in current amplitude after irradiation.

We also measured the effect of UV on the spontaneous currents through OLF channels. CNG channels can open in the absence of ligand, although their open probability under these conditions is extremely low (Picones and Korenbrot, 1995; Ruiz and Karpen, 1997; Tibbs et al., 1997). We used the channels' sensitivity to block by internal divalent ions (Haynes et al., 1986; Stern et al., 1987; Colamartino et al., 1991; Zimmerman and Baylor, 1992) to isolate the currents through unliganded CNG channels. Spontaneous OLF channel currents were obtained as the difference between the patch currents in a control solution lacking cGMP and in an otherwise identical solution containing 10 mM Mg^{2+}. This leak subtraction protocol allowed us to measure the currents through unliganded OLF channels without interference from other sources such as the UV-activated conductance (Middendorf et al., 2000). At this concentration, Mg^{2+} completely blocked the current through OLF channels, but reduced the UV-activated conductance by only ~15%, and had no detectable effect on the leakage conductance of the seal (data not shown).

Exposure to 9.49×10^9 photons $\cdot$ μm^{-2} increased the spontaneous currents through OLF channels in one patch by a factor of ~30 (Fig. 15 A), but decreased the same patch's current at saturating cGMP by 30% (B). UV dose–response relations from similar experiments on five patches are displayed in Fig. 15 C. To facilitate comparison between results from different patches, the spontaneous currents are expressed as a fraction of the patch's current in saturating cGMP before irradiation. On average, a UV dose of 2×10^{10} photons $\cdot$ μm^{-2} increased the spontaneous current by a factor of 28.9 ± 12.1 (mean ± SEM). The same UV dose typically reduced the current in saturating cGMP by ~50% (Table I). Fitting the combined results in Fig. 15 C with Eq. 13 yielded estimates of 2.4×10^{10} photons $\cdot$ μm^{-2} for $D_{1/2}$ and 1.29 for the slope factor. The current asymptote estimated from the fit was $M = 67$, which is only 6% of the maximum possible value [$1/P_o(0) = 1{,}087$].

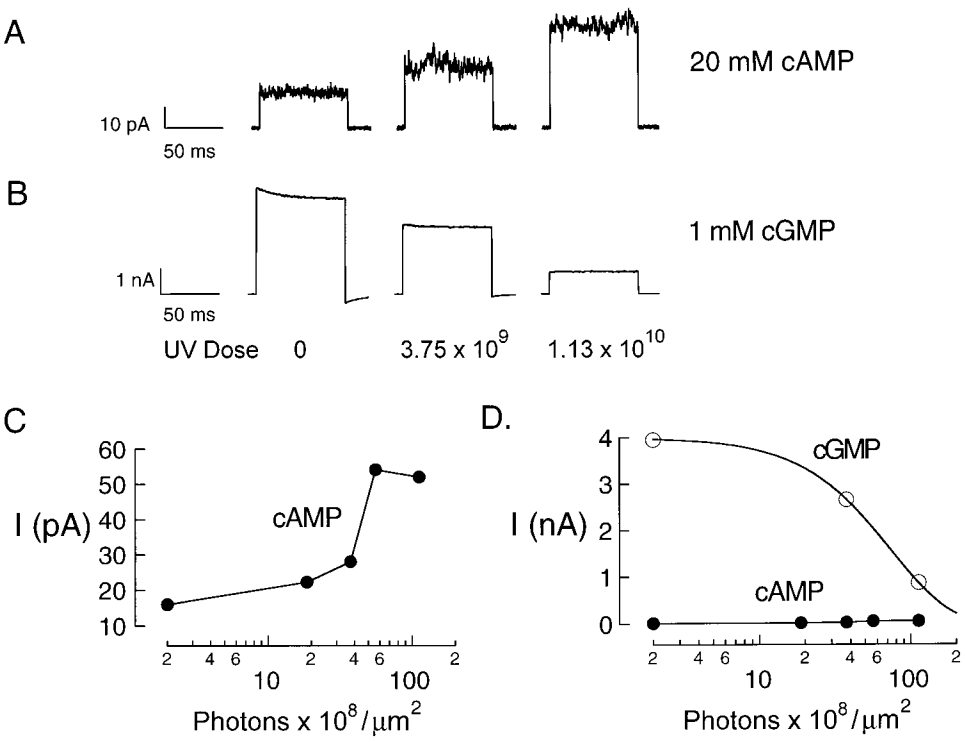

Figure 14. Opposite effects of UV light on currents through RET channels activated by saturating concentrations of cAMP and cGMP. (A) UV effect on current amplitude for RET channels activated by saturating (20 mM) cAMP. Current amplitudes were 17.2, 30.5, and 49.3 pA after cumulative UV doses of 0, 3.75×10^9 and 1.13×10^{10} photons $\cdot$ μm^{-2} at 280 nm. (B) UV effect on current amplitude for RET channels activated by saturating (1 mM) cGMP. Current amplitudes were 4,150, 2,660, and 883 pA after the same UV doses as in A. Note difference in vertical scales for traces in A and B, which are from the same patch. (C) UV dose–response relation for channels activated by saturating cAMP. Patch current in 20 mM cAMP (●) is plotted as a function of UV dose on a semilogarithmic scale. Solid lines connect the experimental points. (D) UV dose–response relation for channels activated by saturating cGMP. Patch current in 1 mM cGMP (○) for results in B is plotted as a function of UV dose on a semilogarithmic scale. Continuous curve is a fit to the results using Eq. 3 with $D_{1/2} = 3.75 \times 10^9$ photons $\cdot$ μm^{-2} and $n^* = 1.6$. Results from C (●) are shown on the same scale for comparison. Note the difference in vertical scales for C and D.

The currents activated by saturating cGMP before UV and the spontaneous currents after UV were blocked by similar concentrations of internal Mg^{2+} ions (Fig. 15 D), providing further verification that the increased currents after irradiation were through unliganded CNG channels.

Fits of the results with a Langmuir single binding isotherm (Eq. 17):

$$\frac{I(\mathrm{Mg})}{I} = \frac{K_i}{[\mathrm{Mg}^{2+}] + K_i}, \qquad (17)$$

yielded inhibition constants (K_i) of 201 ± 23 μM for the spontaneous currents after UV and 350 ± 43 μM for the cGMP-activated currents before UV. The small difference in the K_i values may reflect a weak state dependence to the block, or may indicate that the binding site for internal Mg^{2+} is affected slightly by UV modification of the channels. The latter possibility could be tested by measuring the affinity for Mg^{2+} block of cGMP-activated currents after irradiation.

In summary, UV increased the currents through four channel/ligand pairs with low initial P_o values: RET and OLF channels activated by low concentrations of cGMP (Figs. 1 and 2, respectively), RET channels activated by saturating cAMP (Fig. 14), and OLF channels in the absence of ligand (Fig. 15). For the first three of these pairs, the channels' average initial open probability was on the order of 1%, and UV increased the current in each case by about a factor of 5. The open probability of unliganded OLF channels is ~10-fold lower (~0.1%, see Table II), and the fractional increase in current after a saturating UV dose was ~10-fold higher (~70). For each of the four channel/ligand combinations, the fractional current increase after a saturating UV dose correlated inversely with the channels' initial open probability, as predicted by the energy additive model, but was significantly less than the maximum possible value of $M = 1/P_o(0)$ (Fig. 13, C and D). The UV dose–response relation for unliganded OLF channels was shifted to the right on the abscissa and was steeper than that for RET channels activated by saturating cAMP. The observed changes in the curves' horizontal positions, slopes, and limiting current asymptotes as $\Delta G^0(0)$ was varied are most consistent with the simulations for Case V of the energy additive model, with $n = 1$ (Fig. 13 C) and Case VI, with $n = 10$ (D). We conclude that (a) UV increased the currents through RET and OLF channels by increasing P_o, and (b) the free energy change associated with modification of (−) targets is comparable in magnitude with $|\Delta G^0(0)|$ if the channels contain only a few (−) targets, but $\Delta\Delta G^0(1-)$ may be significantly smaller than $|\Delta G^0(0)|$ if the number of (−) targets is closer to 10 per subunit. The results are clearly

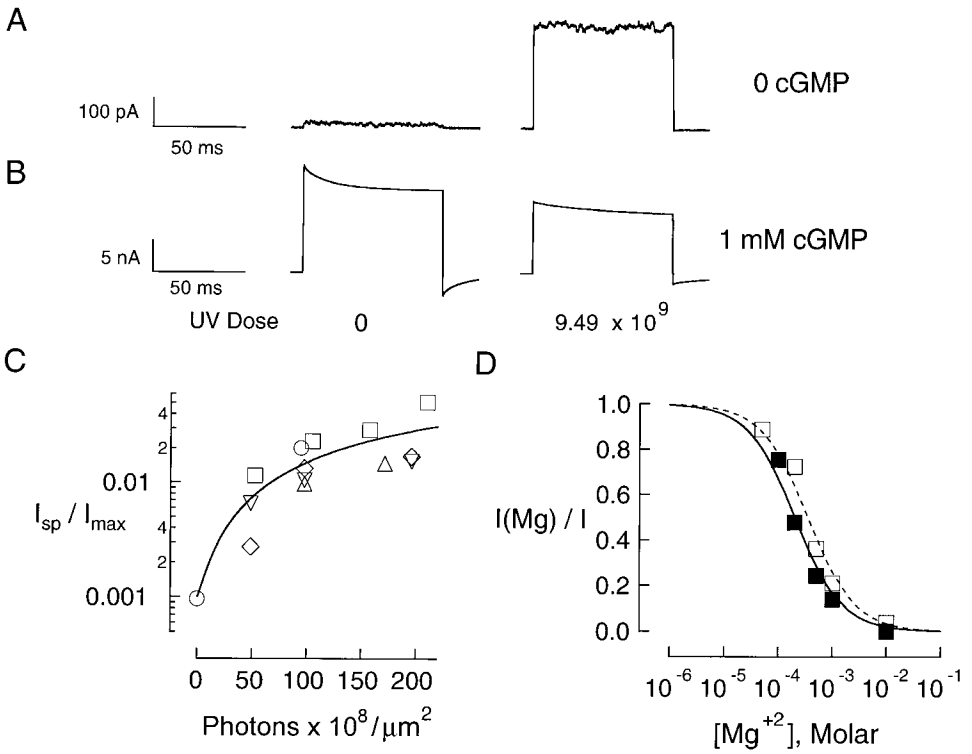

Figure 15. Differential effect of UV light on spontaneous and cGMP-activated currents. (A and B) UV dose dependence of currents through wild-type OLF channels in the absence of cGMP (A) and in the presence of saturating (1 mM) cGMP (B). Current amplitudes before UV exposure and after a UV dose of 9.49×10^9 photons $\cdot \mu m^{-2}$ were 12.3 and 353 pA in the absence of cGMP, and 16.2 and 11.2 nA in 1 mM cGMP. Spontaneous currents were taken as the difference between the currents in standard NaCl control solutions lacking cGMP with and without 10 mM $MgCl_2$. Note the difference in vertical scales for traces in A and B, which are from the same patch. Channels were irradiated with 280 nm UV in the absence of ligand. (C) UV dose–response relation for spontaneous OLF channel currents. Collected results from five patches showing spontaneous current as a function of UV dose on a semi-logarithmic scale. To facilitate comparison between different patches, the spontaneous current for each patch, I_{sp}, was normalized by the maximal current in 1 mM cGMP for the same patch before UV, I_{max}. The continuous curve is a fit to the results using the modified all-or-none model (Eq. 13) with $n^* = 1.29$ and $M = 67$. (D) Block by Mg^{2+} of cGMP-activated currents and UV-induced spontaneous currents. The fraction of unblocked current is plotted as a function of added $MgCl_2$ for currents through OLF channels activated by 1 mM cGMP before UV exposure (□) and spontaneous currents through OLF channels after exposure to 9.49×10^9 photons $\cdot \mu m^{-2}$ at 280 nm (■). Results are from different patches. Smooth curves show fits to the results using Eq. 17. The inhibition constants were 350 ± 43 μM for channels activated by 1 mM cGMP (dotted line), and 201 ± 23 μM for channels activated spontaneously after UV (solid line).

inconsistent with $-\Delta\Delta G^0(1)$ being much larger than $|\Delta G^0(0)|$, regardless of the number of targets.

Modeling the Two Opposing Effects of UV

The net effect of UV light on CNG channel currents depended on the channels' initial open probability. UV always decreased the current when the channels' initial open probability was high (Figs. 1 A, 2 A, 3, 5–7, 10, and 12), and always increased the current when $P_o(0)$ was very low (Figs. 1 B, 2 B, 14, and 15). Why does the sign of the change in current after UV vary if all of the channels contain both (+) and (−) targets that are modified randomly by UV? In some cases, the current amplitude in a given patch changed in opposite directions depending on the "readout" conditions employed (compare Figs. 1, 2, 14, and 15). The opposing changes in current occurred after exposure to similar UV doses, arguing against a large difference in the quantum yields for modifying the (+) and (−) targets. The results are not explained by a difference in the state dependence of these quantum yields either, since the channels were always irradiated in the absence of ligand.

To understand this complex behavior, it was necessary to consider the combined effects of modifying both types of targets in the same channels. To this end, we expanded the energy additive model (Eq. 6) to include (+) and (−) targets. For simplicity, the two types of targets were assumed to be independent, so that the free energy changes associated with their modification were additive. The UV dose–response relation for the expanded energy additive model is given by:

$$\frac{I(D)}{I(0)} = \sum_{k_+=0}^{4(n+)} f(k_+, D) \sum_{k_-=0}^{4(n-)} f(k_-, D) \cdot \frac{1 + \exp[\Delta G^0(0)]}{1 + \exp[\Delta G^0(0) + k_+ \Delta\Delta G^0(1+) + k_- \Delta\Delta G^0(1-)]}. \quad (18)$$

The symbols in Eq. 18 are analogous to those in Eqs. 6 and 7, except for the inclusion of subscripts specific to the (+) and (−) targets.

Fig. 16 shows simultaneous fits of the expanded energy additive model to the results from Figs. 5–7, 14, and 15. The quality of the fits is gratifying, given the relative simplicity of the model. Though not correct in all details, the fits reproduce the main features of the experimental results, including the sign of the changes in current amplitude after irradiation, and the approxi-

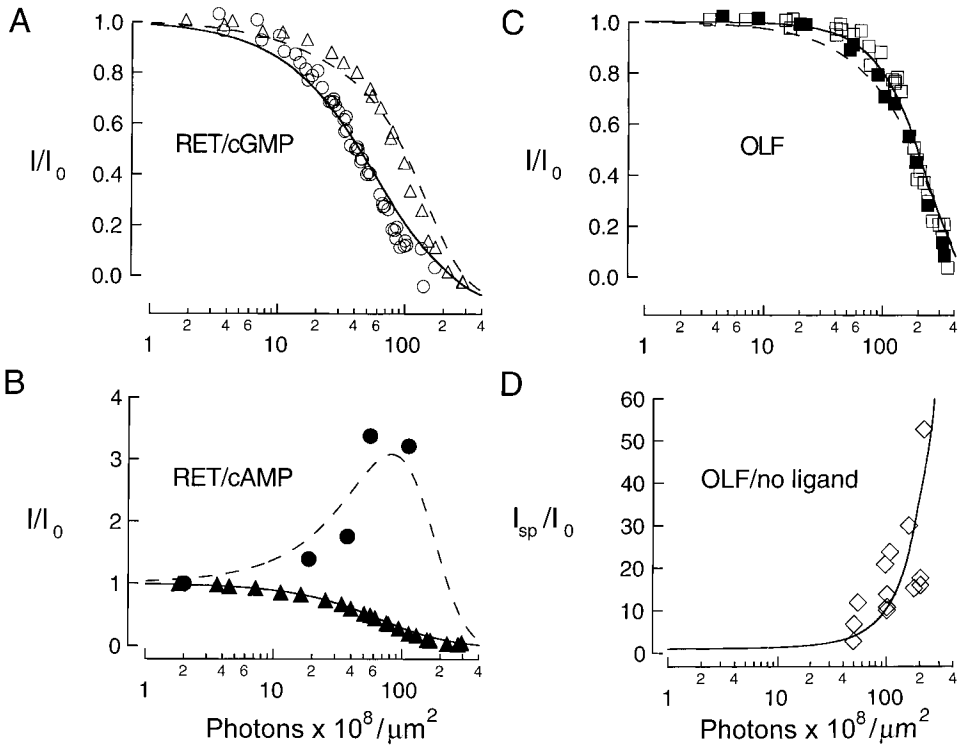

Figure 16. Analysis of UV effects on CNG channels using the expanded energy additive model. (A–D) UV dose–response relations for: (A) RET channels activated by saturating (1 mM) cGMP in the presence (△) and absence (○) of 10 μM cytoplasmic Ni^{2+}. (B) RET channels activated by saturating cAMP (1 mM) in the presence of 10 μM cytoplasmic Ni^{2+} (▲) and saturating (20 mM) cAMP in the absence of Ni^{2+} (●). (C) OLF channels activated by saturating (1 mM) cAMP (■) and saturating (1 mM) cGMP (□). (D) OLF channels with no ligand present (◇). The smooth curves show simultaneous fits to the results in A–D using the expanded energy additive model (Eq 18). The fitted curves were calculated assuming three (+) targets and two (−) targets per channel subunit; however, the results were fit equally well for other target numbers. $\Delta G^0(0)$ values used in the fits are listed in Table II. The quantum yield for each type of target was constrained to be the same for all channel/ligand combinations, and the values obtained from the fits were $\phi_+ = 0.006$ and $\phi_- = 0.02$. The free energy costs for modifying the (+) and (−) targets were allowed to vary for the different channel/ligand combinations. The values of $\Delta\Delta G^0(1+)$ and $\Delta\Delta G^0(1-)$ obtained from the fits were (RT units): for RET/cGMP, +8 and −0.95; for RET/cAMP, +7 and −0.95; for OLF/cGMP, +4.8 and −0.7; for OLF/cAMP, +3 and −0.7; and for OLF/no ligand, 0 and −0.7.

mate relative slopes, horizontal positions, and current asymptotes of the UV dose–response relations for all conditions studied. The model even duplicated the opposite changes in current amplitude that occurred in some cases after the same UV dose when the channels were activated under different conditions (Fig. 16 B). The fitting procedure made the interesting prediction that the UV dose–response relation of RET channels in saturating cAMP is actually biphasic. The current was predicted to reach a maximum after exposure to $\sim 8 \times 10^9$ photons $\cdot$ μm^{-2}, and then to decrease after additional UV (Fig. 16 B). It will be interesting to test this prediction experimentally.

The estimated values of $\Delta\Delta G^0$ for the (+) targets followed the same trends as those obtained from the fits using Eq. 6 (Fig. 9): $\Delta\Delta G^0(1+)$ was about twice as large for RET channels as for OLF channels activated by the same ligand, and was somewhat larger for a given channel activated by cGMP than by cAMP. The magnitude of $\Delta\Delta G^0(1+)$ for each channel/ligand combination was somewhat larger than that estimated using the simpler version of the model (Eq. 6), presumably because modification of the (−) targets partially offsets the free energy deficit caused by modification of the (+) targets. The estimated values of $\Delta\Delta G^0(1-)$ were similar for all channel/ligand combinations studied.

The estimates for $\Delta\Delta G^0$ and ϕ were not unique, since they depended on the (unknown) number of (+) and (−) targets in the channels. We assumed (arbitrarily) that RET and OLF channels contain three (+) targets and two (−) targets per subunit. Increasing the number of either type of target had the effect of decreasing the corresponding quantum yield, similar to the effects observed earlier (Fig. 9 D). The values of the fitting parameters are given in the legend to Fig. 16.

The fits in Fig. 16 provide a possible explanation for why UV decreased the current under some activation conditions but increased the current under other conditions. First, consider the effect of UV on channels with a high initial open probability. Modification of the channels' (−) targets may increase the current through such channels by at most a factor of $1/P_o(0)$ (see above), which is a small factor for $P_o(0) \approx 1$. On the other hand, modification of the channels' (+) targets may reduce the current to a small fraction of its initial value, and therefore dominates the UV effect on the patch current. The situation is very different if the channels' initial open probability is very low. In this case, modification of the channels' (−) targets may increase the current amplitude by a very large factor, since $1/P_o(0)$ represents a 100–1,000-fold enhancement for some of the experimental conditions em-

ployed (Table II). The current through the channel subpopulations that contain many modified (−) targets, but few modified (+) targets therefore dominates the UV effect, leading to the observed increase in macroscopic current.

The simulations in Fig. 16 confirm these ideas quantitatively. For example, only ~15% of the RET channels are estimated to carry over 85% of the current activated by saturating cAMP after a dose of 100×10^8 photons · μm^{-2} (Fig. 16 B). This dominant component of the current was carried by channels with two to six modified (−) targets, but no modified (+) targets. On average, UV increased the current through this subpopulation of channels by a factor of 25. For this same channel/ligand combination in the presence Ni^{2+}, $P_o(0)$ is much higher (≈0.8), and the effect of modifying the (−) targets is small [$1/P_o(0) = 1.25$]. Therefore, modification of the (+) targets dominates under these conditions, and UV decreases the macroscopic currents.

Modeling the UV Effect on the Ligand Dose–Response Relation

As shown in Fig. 16, the expanded energy additive model accounted successfully for the disparate effects of UV on the currents through unliganded and fully liganded CNG channels. However, modeling the UV effect on channel currents over the full range of cGMP concentrations tested (Figs. 1 C and 2 C) required a general theory relating channel open probability to ligand concentration and UV dose. This general theory was obtained by combining various models for CNG channel activation gating with the expanded energy additive model (Eq. 18).

We only considered activation models that include unliganded openings, a well-documented phenomenon (Kramer et al., 1994; Picones and Korenbrot, 1995; Ruiz and Karpen, 1997; Tibbs et al., 1997). Cyclic allosteric models incorporate this feature, yet are conceptually simple and are consistent with many other features of CNG channel gating (Goulding et al., 1994; Varnum and Zagotta, 1996; Liu et al., 1998). Although these models do not account for the multiple subconductance states observed in single RET channel patches (Ruiz and Karpen, 1997, 1999), they are consistent with the ligand dose–response relations of single OLF channels (Liu et al., 1998) and the macroscopic behavior of RET channels (Goulding et al., 1994; Varnum and Zagotta, 1996).

Cyclic allosteric gating models are built upon three basic assumptions. First, it is assumed that the channels contain "gating units" that interconvert between two conformations in a single, concerted step. We use the generic term "gating units" here because the subunit composition of a gating unit differs for different cyclic allosteric models. The two possible conformations of the gating units are denoted as T ("tense") and R ("relaxed"), in reference to the conformations of the hemoglobin molecule (Monod et al., 1965). For ion channels, the T and R states correspond to resting and activated conformations of the gating units, respectively. Since CNG channels are tetramers (Liu et al., 1996; Morrill and MacKinnon, 1999), symmetry considerations suggest that each gating unit contains either one, two, or four channel subunits. We consider the simplest cyclic allosteric model for each of these possibilities. The Hodgkin-Huxley model (HH model) (Hodgkin and Huxley, 1952) assumes that the channels contain four independent gating units, each composed of a single channel subunit (Fig. 17 A). The coupled dimer model (CD model) (Liu et al., 1998) assumes that the channels contain two independent gating units, each consisting of two channel subunits (Fig. 17 B). Finally, the Monod-Wyman-Changeux model (MWC model) (Monod et al., 1965) assumes that the entire channel is a single gating unit composed of four subunits (Fig. 17 C). The second assumption of the cyclic allosteric models is that the gating units interconvert between the T and R conformations in the presence or absence of ligand. Finally, the activating ligand may bind to the T and R conformations of a gating unit with different affinities (denoted K_T and K_R, respectively). Let L denote the equilibrium constant relating the two conformations of an unliganded gating unit: $L = [T]/[R]$. Thermodynamic coupling between the different liganded states of each gating unit changes the equilibrium constant for a gating unit that contains m bound ligands to $c^m \cdot L$, where $c = K_R/K_T$.

The appendix derives general relations for the combined dependence of CNG channel open probability on UV dose and ligand concentration for three models that combine the HH, CD, or MWC schemes with the expanded energy additive model (Eq. 18). In these hybrid models, UV alters P_o by changing the values of the gating parameters c, L, and K_R. The UV dose dependences of these parameters are quantified by replacing the phenomenological (+) and (−) targets of the expanded energy additive model with c, L, and K_R targets, and associating a quantum yield and a free energy cost with their modification (see Eqs. A3–A5).

Since UV increased the current through unliganded OLF channels (Fig. 15), the free energy cost for modifying an L target must be negative (see Eq. A8). This finding, coupled with the observation that UV decreased the current through OLF channels in saturating cGMP, implies that the free energy cost for modifying a c target is positive (see Eq. A9). In other words, UV modification of L targets enhances spontaneous channel opening, while modification of c targets disrupts the coupling between ligand binding and channel opening.

The ligand dose–response relations of RET channels before and after UV were fit using each of the three hybrid UV-cyclic allosteric models (Fig. 17, D–F). The ini-

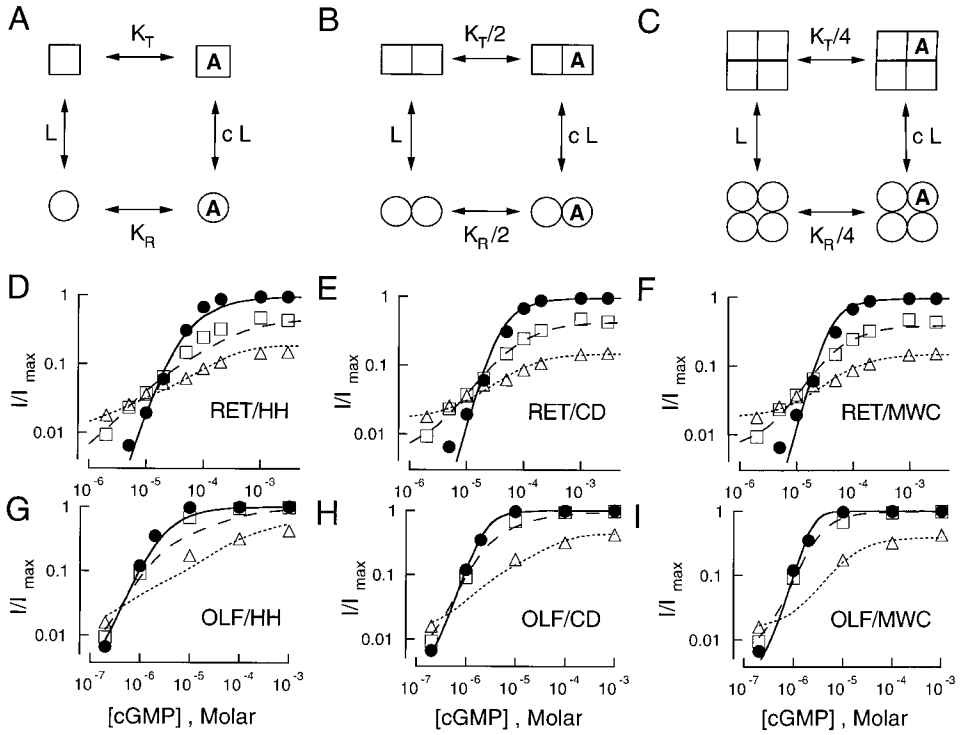

Figure 17. Analysis of UV effect on ligand dose–response relation. (A–C) Schematic depiction of channel activation in: (A) Hodgkin-Huxley, (B) coupled dimer, and (C) Monod-Wyman-Changeux cyclic allosteric activation models. Each panel depicts binding of a single ligand molecule (denoted by A) to a channel gating unit (defined in text). Channel gating units may occupy a resting (T) conformation (squares), or an activated (R) conformation (circles). In the absence of ligand, the conversion between T and R conformations is described by the equilibrium constant L (=[T]/[R]). Ligand binding alters the conversion from the T to the R conformation by the factor c, where $c = K_R/K_T$ is the ratio of ligand binding affinities for the R and T conformations. (D–F) Experimental and calculated ligand dose–response relations for RET channels activated by cGMP before and after UV. Results and symbols are the same as in Fig. 1 C. Smooth curves are fits of the hybrid UV-cyclic allosteric models to the relations before UV (solid line), and after cumulative UV doses of 4.91×10^9 photons · μm^{-2} (long-dashed line), and 9.82×10^9 photons · μm^{-2} (short-dashed line). The calculated curves were computed using Eqs. A1 and A7 for the UV-HH model, with $b = 4$ (D), the UV-CD model with $b = 2$ (E), and the UV-MWC model with $b = 1$ (F). The channels were assumed to contain three c and two L targets per subunit (see text). The following parameter values were used: (D) $K_R = 1.0 \times 10^{-6}$ M, $L = 18.6$, $c = 6.7 \times 10^{-4}$, $\phi_L = 0.101$, $\phi_c = 0.027$, $\Delta\Delta G^0(1L) = -1.19\ RT$, and $\Delta\Delta G^0(1c) = +3.78\ RT$; (E) $K_R = 1.57 \times 10^{-6}$ M, $L = 382$, $c = 8.1 \times 10^{-3}$, $\phi_L = 0.114$, $\phi_c = 0.062$, $\Delta\Delta G^0(1L) = -1.07\ RT$, and $\Delta\Delta G^0(1c) = +1.91\ RT$; and (F) $K_R = 1.52 \times 10^{-6}$ M, $L = 1.47 \times 10^5$, $c = 2.4 \times 10^{-2}$, $\phi_L = 0.129$, $\phi_c = 0.110$, $\Delta\Delta G^0(1L) = -1.03\ RT$, and $\Delta\Delta G^0(1c) = +1.20\ RT$. (G–I) Experimental and calculated ligand dose–response relations for OLF channels activated by cGMP before and after UV. Results and symbols are the same as in Fig. 2 C. Smooth curves are fits to the relations before UV (solid line), and after cumulative UV doses of 4.91×10^9 photons · μm^{-2} (long-dashed line), and 1.96×10^{10} photons · μm^{-2} (short-dashed line). The calculated curves were computed as described for D–F. Parameter values were: (G) $K_R = 1.91 \times 10^{-7}$ M, $L = 4.74$, $c = 2.6 \times 10^{-6}$, $\phi_L = 0.028$, $\phi_c = 0.010$, $\Delta\Delta G^0(1L) = -0.58\ RT$, and $\Delta\Delta G^0(1c) = +3.98\ RT$; (H) $K_R = 3.19 \times 10^{-7}$ M, $L = 32$, $c = 8.8 \times 10^{-4}$, $\phi_L = 0.045$, $\phi_c = 0.014$, $\Delta\Delta G^0(1L) = -0.41\ RT$, and $\Delta\Delta G^0(1c) = +3.88\ RT$; and (I) $K_R = 4.11 \times 10^{-7}$ M, $L = 1088$, $c = 1.5 \times 10^{-2}$, $\phi_L = 0.069$, $\phi_c = 0.027$, $\Delta\Delta G^0(1L) = -0.36\ RT$, and $\Delta\Delta G^0(1c) = +1.66\ RT$.

tial value of L for each cyclic allosteric model was estimated from the channels' spontaneous open probability, P_{sp}, using the relation:

$$L = \frac{1-(P_{sp})^{1/a}}{(P_{sp})^{1/a}}. \quad (19)$$

In Eq. 19, the parameter a denotes the number of gating units in a channel. The initial value of the gating parameter c for each model was computed from P_{sp} and the open probability in saturating cGMP, P_{max} (see Table II), using the relation:

$$c = \left[\frac{1-(P_{max})^{1/a}}{1-(P_{sp})^{1/a}}\right]^{a/4}\left[\frac{P_{sp}}{P_{max}}\right]^{1/4}. \quad (20)$$

Eqs. 19 and 20 were obtained by considering the limiting behavior of Eqs. A1 and A2 (see appendix), and making the simplifying assumption that the channels are open only when all of their gating units are in the activated conformation. The initial value of K_R for each model was determined by fitting the cGMP dose–response relation before UV, using Eqs. A1 and A2 and the initial values of c and L determined from Eqs. 19 and 20.

The post-UV ligand dose–response relations were fit simultaneously using Eqs. A1 and A7, with the quantum yields and free energy costs of the L and c targets as the only adjustable parameters. The results of Middendorf et al. (2000) did not provide a specific estimate for the number of targets in the channels, but did suggest that the number is small. We assumed (arbitrarily) that the channels contain three c targets and two L targets. The cGMP dose–response relations of OLF channels before and after UV were analyzed by the same procedure.

Fig. 17, D–I, shows the fits of the hybrid UV-cyclic allosteric models to the ligand dose–response relations of

RET and OLF channels before and after UV. The simulated curves for all three models reproduced the general features of the results, including the magnitude of the current reduction in saturating cGMP, the magnitude of the current increase at very low cGMP concentration, and the shallower slopes of the relations after UV. Due to the complexity of the computations, we did not systematically explore the effects of varying the number of *c* and *L* targets. However, since the results could be fit using other target numbers (not shown), the UV parameters obtained from the fits are not unique. The results were fit equally well by the UV-MWC and UV-CD hybrid models, but less well by the UV-HH model. Other simulations (not shown) indicate that a "best" model might be identified from the three hybrid models if independent estimates were available for the number or quantum yields of the UV targets. The values of the fitting parameters are given in the legend to Fig. 17.

DISCUSSION

Mechanism of Current Alteration by UV

UV light had variable effects on the currents through CNG channels. The channels' initial open probability determined the sign of the change in current after irradiation. UV decreased the current through channels with high initial open probabilities [$P_o(0) > 0.3$; Figs. 1 A, 2 A, 3, 5–7, 10, and 12], but had the opposite effect on channels with low initial open probability values [$P_o(0) < 0.02$; Figs. 1 B, 2 B, 14, and 15]. These effects of UV could not be attributed to variability in the measurements, as the dose dependence of channel current was highly reproducible for each set of experimental conditions (see, for example, Fig. 5). Furthermore, the opposite effects of UV on channel current were observed in many cases within the same patch (Figs. 1, 2, 14, and 15).

The expanded energy additive model (Eq. 18) accounted successfully for the UV effects on the channel currents for all conditions studied (Fig. 16). This model assumes that the channels contain two distinct types of target residues whose modification exerts opposite and additive effects on the free energy difference between the channels' open and closed states. The next two sections discuss how the presence of the two types of UV targets complicates both the interpretation of the channels' action spectrum (Middendorf et al., 2000) and the identification of the target residues within the channel sequence.

Interpretation of Action Spectrum in Saturating cGMP

The wavelength dependence of the UV sensitivity (the action spectrum) of RET channels activated by saturating cGMP was very similar to the absorption spectrum of tryptophan (Middendorf et al., 2000). Since the initial open probability of RET channels in saturating cGMP is close to one (Table II), and the modification of the (+) targets dominates the UV effect under these conditions (see above), the form of the action spectrum strongly suggests that the (+) targets are tryptophans. It is more difficult to identify the (−) targets from the action spectrum because they make a small contribution to the UV dose–response relation when $P_o(0)$ is close to one (see above). We estimated the relative contributions of the (+) and (−) targets to the UV dose–response relation by calculating the relations with and without (−) targets, using the parameters from the fits in Fig. 16 A. Including the (−) targets in the calculation increased the half-saturating UV dose by only 9%. We then computed the action spectrum that is expected if the (−) targets were tyrosine residues by adding normalized tryptophan and tyrosine absorption spectra together in a 10:1 ratio. The calculated action spectrum was not sufficiently different from the absorption spectrum of tryptophan alone to allow identification of the (−) targets by this method. A more sensitive method for identifying the (−) targets may be to measure the action spectrum of channels with low initial open probabilities, since modification of the (−) targets dominates the UV effect under those conditions (see above).

Identification and Characterization of Target Residues

As described in the preceding paper (Middendorf et al., 2000), one approach to locating the UV targets in the channels is to identify tryptophan residues that alter the channels' UV sensitivity when replaced by other amino acids. This approach assumes that mutating a residue in the channel will alter the channels' UV sensitivity if the residue is a UV target, but have no effect on the UV sensitivity if it is not a UV target. The results in the present paper indicate that mutations may also change the channels' UV sensitivity indirectly by altering their initial open probability (see Fig. 10). The indirect effect may occur even if the replaced tryptophan is not a UV target. The converse is also possible: mutations that replace target tryptophans with other residues may have little or no effect on the channels' UV sensitivity. For example, mutating a (+) target tryptophan to another amino acid will tend to reduce the channels' UV sensitivity by lowering the net absorption cross section of the (+) targets. However, this contribution to the UV sensitivity may be offset if the mutation lowers $P_o(0)$, since the latter effect would tend to increase the channels' UV sensitivity. These arguments indicate that replacing a tryptophan residue by a different amino acid may either increase, decrease, or have no affect on the channels' UV sensitivity, whether the tryptophan is a target residue or not! Clearly, it is incorrect to identify specific tryptophans in the channel se-

quence as targets based solely on changes in the UV sensitivities of mutant channels. Rather, it is important to have a detailed physical model for interpreting UV sensitivity results.

Given the many complicated effects possible in a UV modification experiment, and the difficulty of determining a complete model for the UV effect, could other methods be used to identify the UV targets in CNG channels? An approach that eliminates some of the complications outlined above is to examine the UV sensitivity of CNG channels containing only a single tryptophan residue per subunit. The remaining tryptophan in such a mutant could be identified as a UV target with confidence if the channel was sensitive to UV and its action spectrum had the form of a tryptophan absorption spectrum. The sign of the change in current after irradiation would allow further classification of the tryptophan as a (+) or (−) target. A significant potential problem with this approach is the difficulty of expressing channels with multiple tryptophan replacements. We failed to obtain cGMP-dependent currents from many RET channel mutants that replaced more than one of the channels' 10 native tryptophans with other amino acids (Middendorf et al., 2000). However, the apparent lack of expression was likely due in many cases to a very low open probability of the mutant channels. As we demonstrated for the pore tryptophan mutants (Fig. 10), tryptophan replacements may be tolerated better in the OLF channel due to its more favorable activation properties.

Energetic Contribution of the Pore Tryptophan Residue to Channel Gating and Its Relation to Channel Structure

We found that replacing the pore tryptophan residue by other aromatic amino acids reduced the open probability of OLF channels (Fig. 10) and RET channels (Middendorf et al., 2000) significantly. Using Eqs. 4 and 5 and the results in Fig. 10 D, we estimated the quantitative effect of the pore mutations on the channels' gating energetics. Assuming that the difference between ΔG^0 for the allosteric opening transition in saturating cGMP and cAMP is the same for wild-type OLF and OLF/W332 mutant channels, we estimate that replacing tryptophan 332 by tyrosine (histidine) changed the free energy difference for the allosteric opening transition by approximately +5.4 *RT* (+4.8 *RT*). These energetic changes are similar to the difference in the free energy of the allosteric opening transition for OLF channels activated by saturating cAMP compared with saturating cGMP (approximately +5.3 RT, see Table II), and to the energetic effect of cytoplasmic Ni^{2+} ions on the gating of RET channels in saturating ligand (approximately −5 *RT*; Gordon and Zagotta, 1995a).

The pore tryptophan residue is conserved in all known CNG channels, as well as the related voltage-gated potassium channels (Jan and Jan, 1990) and a proton-gated channel, KcsA, from the bacterium *Streptomyces lividans*. KcsA channels contain two hydrophobic transmembrane regions and an intervening pore sequence that likely corresponds to the S5, pore, and S6 regions of CNG and voltage-gated channels. Recent structural results on KcsA (Doyle et al., 1998; Perozo et al., 1998, 1999) provide a framework for interpreting our results for the pore tryptophan mutants in CNG channels. The conserved tryptophan residue in KcsA channels is located near the COOH-terminal end of the pore helix, a region of the channel that moves during channel opening (Perozo et al., 1999). This residue and the preceding tryptophan residue (which is a tyrosine in CNG channels) form a collar of aromatic amino acids positioned around the channels' selectivity filter (Doyle et al., 1998). The tryptophans in the collar interact with a tyrosine in the selectivity filter via hydrogen bonds, suggesting that the tryptophans may influence its structure. If the structure of KcsA and CNG channels are similar, it is not surprising that altering the sidechain of the pore tryptophan has such a drastic effect on the open probability of CNG channels. Mutation of other residues in the channel pore has also been shown to affect activation gating (Bucossi et al., 1997; Fodor et al., 1997a,b). Our results are consistent with the idea that the pore tryptophans may influence gating by interacting directly with the channel's selectivity filter. It is worth noting that the tyrosine residue in the selectivity filter of KcsA and voltage-gated channels is missing in CNG channels.

UV Sensitivity of Pore Tryptophan Mutants

An alternative explanation for the increased UV sensitivity of OLF/W332Y and OLF/W332H channels (Fig. 10, A and B) is that the pore tryptophan residues are (−) targets. Photochemical modification of W332 would favor channel opening and therefore antagonize the current reduction due to modification of the channels' (+) targets. Replacing the pore tryptophan with a different amino acid would remove this "protective" effect, making the channels more sensitive to UV. We do not favor this idea. It seems unlikely that tryptophan 332 is a (−) target since replacing this residue by similar amino acids such as tyrosine or histidine reduced the channels' open probability (Fig. 10, C and D). As discussed earlier, we favor instead the idea that the pore mutation increased the UV sensitivity of OLF/W332Y and OLF/W332H channels by reducing the channels' initial open probability (Fig. 4). Because conservative mutations of the pore tryptophans reduced the channels' open probability (Fig. 10, C and D), photochemical modification of those residues will likely reduce P_o as well, suggesting that they may actually be (+) targets.

Channel Destruction by UV

Modeling of the UV dose–response relations (Fig. 16) suggests that the free energetic cost of modifying UV targets in CNG channels is comparable in magnitude to the initial free energy difference between the channels' open and closed states. It is possible that some photochemical modifications may exert more drastic effects on the channels, which we will call channel destruction. In those instances, the free energy cost of target modification is much larger than $\Delta G^0(0)$, and a single target modification completely eliminates the channel current. This mechanism of channel destruction by UV is formally equivalent to the all-or-none model described in the preceding paper (Middendorf et al., 2000).

We estimated the maximum possible contribution of channel destruction to the UV effect on CNG channels by comparing the UV dose–response relations of OLF/W332Y and OLF/W332H channels to that of wild-type OLF channels. Since wild-type channels contain one more tryptophan per subunit than the pore mutant channels, the amount of UV-induced destruction of OLF channels represents an upper limit to the amount that may occur in OLF/W332Y and OLF/W332H channels. Furthermore, since $\Delta G^0(0)$ is more negative for the wild-type compared with the mutant channels, a modification that destroyed an OLF channel would necessarily be sufficient to destroy one of the pore mutant channels. A UV dose containing 8.50×10^9 photons $\cdot\ \mu m^{-2}$ reduced the current through OLF channels by only ~10%, but reduced the current through the pore mutant channels by 85–90% (Fig. 10, A and B). This comparison suggests that channel destruction accounts for no more than ~10–20% of the current reduction by UV.

Expected Heterogeneity of Single Channel Records after Irradiation

The idea that UV alters the open probabilities of CNG channels by modifying two distinct types of target residues leads to a number of testable predictions regarding the effect of UV on the currents through single CNG channels. Since UV modification of the targets occurs randomly, the minimal UV dose required to alter the channels' open probability is expected to vary from patch to patch, even for channels containing a single UV target. Analysis of such records for a large number of patches may provide a direct estimate of the targets' photochemical quantum yields.

The expanded energy additive model (Eq. 18) predicts that modification of an individual (+) or (−) UV target in a channel should cause a discrete "jump" in the channel's open probability to a lower or higher value, respectively. The magnitude of the changes in open probability associated with such jumps may provide estimates for the free energy cost of modifying each type of target.

The UV-activated conductances present in oocyte membranes (Middendorf et al., 2000) currently prevent us from measuring UV effects at the single channel level. This problem may be circumvented by identifying compounds that block the UV-activated conductances, or by using an expression system where they are not present.

Using UV Modification to Measure Extremes in Channel Energetics

This section describes how UV modification may be used to measure free energy changes in regimes that were previously inaccessible to accurate measurement. For a channel with a single open and a single closed state, the open probability depends on the standard free energy difference between those states as:

$$P_o = \frac{\exp[-\Delta G^0(0)]}{1 + \exp[-\Delta G^0(0)]}, \quad (21)$$

where $\Delta G^0(0)$ is expressed in RT units. Eq. 21 indicates that small uncertainties in open probability correspond to huge uncertainties in the associated free energy difference when P_o is near unity (Fig. 18 A). Thus, it is difficult in many cases to quantify even large energetic effects on channel gating equilibria because the effect on P_o, the observable quantity in most experiments, is negligible (see Colquhoun, 1998).

Fig. 18 B shows the UV dose–response relation for wild-type OLF channels in saturating cGMP, along with the fit to these results (1) from Fig. 16. The initial free energy difference, $\Delta G^0(0)$, is $-9.9\ RT$ for this channel/ligand pair, which corresponds to an open probability close to unity [$P_o(0) = 0.99995$, Table II]. Fig. 18 B, 2–4, are calculated for hypothetical channels with even larger $\Delta G^0(0)$ values, but the same UV parameters as used for 1. For example, 2–4 might correspond to UV dose–response relations for channels containing mutations that enhance channel opening relative to OLF/cGMP. The hypothetical channels' open probabilities are so close to unity that the energetic effects of the mutations could not be measured by existing methods, such as single channel recording or noise analysis. The simulations indicate that the differences in $\Delta G^0(0)$ for the hypothetical channels would be detected easily by the UV modification method, however.

UV modification may also be useful for investigating channels with very low open probabilities. For example, the activation mechanism of unliganded CNG channels is quite difficult to study because the spontaneous currents are very small (Taylor and Baylor, 1995; Ruiz and Karpen, 1997; Tibbs et al., 1997). Mutant channels that lack (+) targets may provide an ideal system for studying this process. Simulations using Eq. 18 predict that UV should increase the spontaneous open

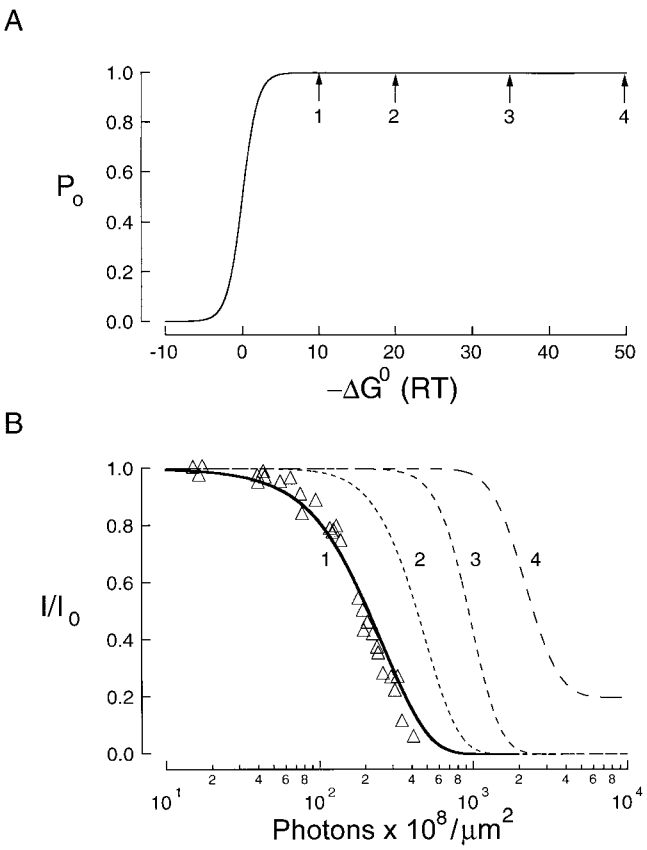

Figure 18. Sensitivity of UV dose–response relation to changes in $\Delta G^0(0)$ that do not significantly alter channel open probability. (A) Nonlinear relation between open probability and standard free energy difference between open and closed channel states, ΔG^0. The smooth curve was computed using Eq. 21. For the various numbered arrows (shown in parentheses), the values of ΔG^0 (RT units) and the corresponding values of $1 - P_o$, were, respectively: (1) -9.9 and 5×10^{-5}, (2) -20 and 2×10^{-9}, (3) -35 and 6×10^{-16}, (4) -50 and 2×10^{-22}. (B) Simulated UV dose–response relations for channels with very different ΔG^0 that all correspond to P_o values near unity. △ show the measured UV dose–response relation for OLF channels activated by saturating (1 mM) cGMP (Fig. 5). The bold curve (1) is the fit to these results using the parameters in Fig. 16 C. The other numbered curves were calculated using the ΔG^0 values corresponding to the equivalent numbered arrows in A, but the same UV parameters as for 1.

probabilities for such mutants into a range where the unliganded openings are easily measured.

Using UV Modification to Test Models for CNG Channel Activation

Studies of channel activation may benefit from the use of multiple methods for simultaneously perturbing gating. For example, quantitative measurements of the combined effects of intracellular Ca^{2+} and membrane voltage on the gating of Ca-activated K (*mSlo*) channels provided significant constraints on activation models for those channels (Cox et al., 1997; Cui et al., 1997; Horrigan and Aldrich, 1999; Horrigan et al., 1999; Rothberg and Magleby, 1999). The UV dose dependence of currents reported here may be useful for investigating the activation mechanism of CNG channels. Like membrane voltage in the example above, UV dose provides a second "axis" for perturbing channel gating that is distinct from changing the ligand concentration. Further characterization of the UV effect will be necessary to understand the combined energetic effects of ligand binding and target modification on channel gating. Since UV modification breaks the symmetry of the channels (see Eq. A6), it may be particularly useful for studying cooperative effects in channel gating.

Relationship to Other Spectroscopic Experiments

Spectroscopic approaches have provided new insights into the mechanism of ion channel gating. Voltage-dependent changes in the emission from channels labeled with fluorescent dyes measure the structural changes associated with gating charge movement and channel opening directly (Mannuzzu et al., 1996; Cha and Bezanilla, 1997; Cha et al., 1999; Glauner et al., 1999). A distinct drawback of this technique is the large size of the fluorescent probe and its maleimide linker, which may alter channel gating and provide a rather poor spatial resolution. Measurements of the emission from the channels' intrinsic tryptophan fluorophores may be useful because they circumvent these limitations. Furthermore, the results in this paper and the preceding paper (Middendorf et al., 2000) indicate that some of the tryptophans in CNG channels are likely located in or near the channels' gating machinery, and thus may report on gating conformational changes.

The relatively high photobleaching quantum yields of protein tryptophans ($\phi \approx 10^{-1}$–10^{-3}) compared with fluorescent dyes ($\phi \approx 10^{-4}$–10^{-6}) poses two problems for channel fluorescence measurements. First, very low light levels and large numbers of channels may be required to prevent significant reduction in the fluorescence signals during the course of an experiment. In addition, we have shown here that photochemical modification of tryptophan residues perturbs channel activation. Thus, it will be very important to ensure that the signals in channel fluorescence experiments originate from channels with unmodified UV targets.

Such experiments may also be useful as a direct method for determining the photochemical quantum yield of the UV targets in CNG channels. Direct measurements of the quantum yields will be useful because they reduce the number of variable parameters needed to fit the UV dose–response relations and may provide additional constraints for testing and refining channel activation models (Fig. 17).

APPENDIX

This section develops a general theory for the combined dependence of CNG channel open probability

on ligand concentration and UV dose. The theory is used in results to analyze the effect of UV light on the cGMP dose–response relations of RET and OLF channels (Fig. 17).

The general theory uses the cyclic allosteric models described above to characterize CNG channel gating in the absence of UV. The fundamental mechanistic similarity of the HH, CD, and MWC models allows the dependence of channel open probability on ligand concentration for all of these models to be expressed by the single equation:

$$P_o([A]) = \sum_{i=b}^{a} \binom{a}{b} \{P_R([A])\}^i \{1 - P_R([A])\}^{(a-i)}. \quad (A1)$$

In Eq. A1, the first term in parentheses is the appropriate binomial coefficient and [A] is the ligand concentration. Factor a is the number of gating units in the channel, which is equal to 4 for the HH model, 2 for the CD model, and 1 for the MWC model. b is the minimum number of gating units that must activate to open the channel, and may assume values of 1, 2, 3, or 4 for the HH model, 1 or 2 for the CD model, and 1 for the MWC model. $P_R([A])$ is the probability that a channel gating unit is in the activated (R) conformation, and is given by:

$$P_R([A]) = \frac{(1+\alpha)^{4/a}}{(1+\alpha)^{4/a} + L(1+c\alpha)^{4/a}}, \quad (A2)$$

where α is equal to $[A]/K_R$.

We combined the expanded energy additive model (Eq. 18) and the cyclic allosteric models by replacing the phenomenological (+) and (−) targets in Eq. 18 with K_R, c, and L targets. By analogy with Eq. 4, UV modification of these targets alters the gating parameters K_R, c, and L according to the relations:

$$K_R(k_K) = K_R(0)\exp[k_K \cdot \Delta\Delta G^0(1K)], \quad (A3)$$

$$c(k_c) = c(0)\exp[k_c \cdot \Delta\Delta G^0(1c)], \quad (A4)$$

and

$$L(k_L) = L(0)\exp[k_L \cdot \Delta\Delta G^0(1L)], \quad (A5)$$

where k_K, k_c, and k_L refer to the number of modified targets of each type, and $\Delta\Delta G^0(1K)$, $\Delta\Delta G^0(1c)$, and $\Delta\Delta G^0(1L)$ denote the corresponding free energy costs (in RT units) of modifying one target of that type. (Note: the minus sign in the argument of the exponential term in Eq. 4 is missing in Eqs. A3–A5 because the convention used in defining K_R, c, and L is opposite that used in Eq. 4.)

Eq. A2 assumes that all of a channels' gating units are identical before irradiation. UV modification of the L, c, and K_R targets in different subunits breaks this functional symmetry. A more general form of Eq. A2 that accounts for the symmetry breaking induced by UV is:

$$P_R([A]) = \prod_{i=1}^{a} \left[\frac{\prod_{j=1}^{4/a}(1+\alpha_{ij})}{\prod_{j=1}^{4/a}(1+\alpha_{ij}) + L_i \prod_{j=1}^{4/a}(1+c_{ij}\alpha_{ij})} \right], \quad (A6)$$

where the index i counts over the gating units of the channel and j counts over the subunit components of the gating units. For example, $i = 1$ and $1 \le j \le 4$ for the MWC model, while $1 \le i \le 2$ and $1 \le j \le 2$ for the CD model. Assuming that the UV targets are modified independently, Eq. A6 may be combined with Eqs. A3–A5 to yield the following expression for P_R as a function of ligand concentration and UV dose:

$$P_R([A], D) = \prod_{i=1}^{a} \cdot$$

$$\frac{\sum_{k_{Li}=0}^{(4n_L/a)} f(k_{Li}, D) \prod_{j=1}^{4/a} \sum_{k_{cij}=0}^{n_c} f(k_{cij}, D)[1 + \alpha_{ij}(k_{Kij})]}{\prod_{j=1}^{4/a}[1 + \alpha_{ij}(k_{Kij})] + L_i(k_{Li}) \prod_{j=1}^{4/a}[1 + c_{ij}(k_{cij})\alpha_{ij}(k_{Kij})]}. \quad (A7)$$

In Eq. A7, k_{Kij}, k_{cij}, and k_{Li} refer to the number of modified K_R, c, and L targets in the subunit identified by the indices i and j, n_c and n_L are the number of c and L targets per subunit, respectively, and the $f(k_{cij}, D)$, and $f(k_{Li}, D)$ factors are analogous to $f(k, D)$ in Eq. 7. Eq. A7 was simplified by assuming that the entire effect of UV on the activation parameter c ($= K_R/K_T$) is due to an effect on K_R; thus, $\Delta\Delta G^0(1K) = \Delta\Delta G^0(1c)$.

What is the correspondence between the molecular free energy parameters $\Delta\Delta G^0(1c)$ and $\Delta\Delta G^0(1L)$ in the cyclic allosteric models and the phenomenological free energy parameters $\Delta\Delta G^0(1+)$ and $\Delta\Delta G^0(1-)$ in the expanded energy additive model (Eq. 18)? It is useful to consider the channels' gating behavior in two limits. In the absence of ligand, Eq. A7 simplifies to:

$$\lim_{A \to 0} P_R([A], D) = \prod_{i=1}^{a} \sum_{k_{Li}=0}^{(4n_L/a)} f(k_{Li}, D) \cdot \left\{ \frac{1}{1 + L(0)\exp[k_{Li} \cdot \Delta\Delta G^0(1L)]} \right\}. \quad (A8)$$

Factors related to K_R and c do not appear in Eq. A8 because the spontaneous open probability depends only on L for the cyclic allosteric models. Since UV increased the spontaneous currents through OLF chan-

nels (Fig. 15), $\Delta\Delta G^0(1L)$ is negative. For a saturating concentration of ligand, Eq. A7 reduces to:

$$P_R([A], D) = \prod_{i=1}^{a} \frac{\sum_{k_{Li}=0}^{(4n_L/a)} f(k_{Li}, D) \prod_{j=1}^{4/a} \sum_{k_{cij}=0}^{n_c} f(k_{cij}, D)}{1 + L_i(k_{Li}) \prod_{j=1}^{4/a} c_{ij}(k_{cij})}, \quad \text{(A9)}$$

indicating that the current after irradiation depends on both c and L. Since $\Delta\Delta G^0(1L)$ is negative and UV decreased the current through OLF channels activated by 1 mM cGMP, $\Delta\Delta G^0(1c)$ must be positive.

The authors thank Denis Baylor and Dan Cox for helpful discussions, Denis Baylor and Laura Mazzola for critical reading of the manuscript, and Robert Schneeveis for excellent technical assistance.

This work was supported by grants from the National Institutes of Health (NS23294), the National Eye Institute (EY01543), and the McKnight Foundation. R.W. Aldrich is an investigator with the Howard Hughes Medical Institute.

Submitted: 27 March 2000
Revised: 1 June 2000
Accepted: 5 June 2000

REFERENCES

Ahmad, I., C. Korbmacher, A.S. Segal, P. Cheung, E.L. Boulpaep, and C.J. Barnstable. 1992. Mouse cortical collecting duct cells show nonselective cation channel activity and express a gene related to the cGMP-gated rod photoreceptor channel. *Proc. Natl. Acad. Sci. USA.* 89:10262–10266.

Bezanilla, F., E. Perozo, and E. Stefani. 1994. Gating of *Shaker* K^+ channels: II. The components of gating currents and a model of channel activation. *Biophys. J.* 66:1011–1021.

Biel, M., X. Zong, M. Distler, E. Bosse, N. Klugbauer, M. Murakami, V. Flockerzi, and F. Hofmann. 1994. Another member of the cyclic nucleotide-gated channel family, expressed in testis, kidney, and heart. *Proc. Natl. Acad. Sci. U. S. A.* 91:3505–3509.

Brown, R.L., S.D. Snow, and T.L. Haley. 1998. Movement of gating machinery during the activation of rod cyclic nucleotide-gated channels. *Biophys. J.* 75:825–833.

Bucossi, G., M. Nizzari, and V. Torre. 1997. Single-channel properties of ionic channels gated by cyclic nucleotides. *Biophys. J.* 72: 1165–1181.

Cha, A., and F. Bezanilla. 1997. Characterizing voltage-dependent conformational changes in the *Shaker* K^+ channel with fluorescence. *Neuron*. 19:1127–1140.

Cha, A., G.E. Snyder, P.R. Selvin, and F. Bezanilla. 1999. Atomic scale movement of the voltage-sensing region in a potassium channel measured via spectroscopy. *Nature.* 402:809–813.

Coburn, C.M., and C.I. Bargmann. 1996. A putative cyclic nucleotide-gated channel is required for sensory development and function in *C. elegans*. *Neuron*. 17:695–706.

Colamartino, G., A. Menini, and V. Torre. 1991. Blockade and permeation of divalent cations through the cyclic GMP-activated channel from tiger salamander retinal rods. *J. Physiol.* 440:189–206.

Colquhoun, D. 1998. Binding, gating, affinity and efficacy: the interpretation of structure–activity relationships for agonists and of the effects of mutating receptors. *Br. J. Pharmacol.* 125:924–947.

Cox, D.H., J. Cui, and R.W. Aldrich. 1997. Allosteric gating of a large conductance Ca-activated K^+ channel. *J. Gen. Physiol.* 110: 257–281.

Creighton, T.E. 1993. Proteins: Structures and Molecular Properties. 2nd ed. W.H. Freeman & Co., New York, NY. 507 pp.

Cui, J., D.H. Cox, and R.W. Aldrich. 1997. Intrinsic voltage dependence and Ca^{2+} regulation of mslo large conductance Ca-activated K^+ channels. *J. Gen. Physiol.* 109:647–673.

Dhallan, R.S., K.W. Yau, K.A. Schrader, and R.R. Reed. 1990. Primary structure and functional expression of a cyclic nucleotide-activated channel from olfactory neurons. *Nature.* 347:184–187.

Ding, C., E.D. Potter, W. Qiu, S.L. Coon, M.A. Levine, and S.E. Guggino. 1997. Cloning and widespread distribution of the rat rod-type cyclic nucleotide-gated cation channel. *Am. J. Physiol. Cell Physiol.* 272:C1335–C1344.

Doyle, D.A., J.M. Cabral, R.A. Pfuetzner, A. Kuo, J.M. Gulbis, S.L. Cohen, B.T. Chait, and R. MacKinnon. 1998. The structure of the potassium channel: molecular basis of K^+ conduction and selectivity. *Science.* 280:69–77.

Finn, J.T., J. Li, and K.-W. Yau. 1995. C-terminus involvement in the gating of cyclic nucleotide- activated channels in rod photoreceptors. *Biophys. J.* 68:A253. (Abstr.)

Fodor, A.A., K.D. Black, and W.N. Zagotta. 1997a. Tetracaine reports a conformational change in the pore of cyclic nucleotide–gated channels. *J. Gen. Physiol.* 110:591–600.

Fodor, A.A., S.E. Gordon, and W.N. Zagotta. 1997b. Mechanism of tetracaine block of cyclic nucleotide-gated channels. *J. Gen. Physiol.* 109:3–14.

Glauner, K.S., L.M. Mannuzzu, C.S. Gandhi, and E.Y. Isacoff. 1999. Spectroscopic mapping of voltage sensor movement in the *Shaker* potassium channel. *Nature.* 402:813–817.

Gordon, S.E., M.D. Varnum, and W.N. Zagotta. 1997. Direct interaction between amino- and carboxyl-terminal domains of cyclic nucleotide–gated channels. *Neuron*. 19:431–441.

Gordon, S.E., and W.N. Zagotta. 1995a. A histidine residue associated with the gate of the cyclic nucleotide-activated channels in rod photoreceptors. *Neuron*. 14:177–183.

Gordon, S.E., and W.N. Zagotta. 1995b. Localization of regions affecting an allosteric transition in cyclic nucleotide–activated channels. *Neuron*. 14:857–864.

Goulding, E.H., J. Ngai, R.H. Kramer, S. Colicos, R. Axel, S.A. Siegelbaum, and A. Chess. 1992. Molecular cloning and single-channel properties of the cyclic nucleotide–gated channel from catfish olfactory neurons. *Neuron*. 8:45–58.

Goulding, E.H., G.R. Tibbs, and S.A. Siegelbaum. 1994. Molecular mechanism of cyclic-nucleotide–gated channel activation. *Nature.* 372:369–374.

Grossweiner, L.I. 1976. Photochemical inactivation of enzymes. *Curr. Top. Radiat. Res. Q.* 11:141–199.

Haynes, L.W., A.R. Kay, and K.-W. Yau. 1986. Single cyclic GMP–activated channel activity in excised patches of rod outer segment membrane. *Nature.* 321:66–70.

Hodgkin, A.L., and A.F. Huxley. 1952. A quantitative description of membrane current and its application to conduction and excitation in nerve. *J. Physiol.* 117:500–544.

Horrigan, F.T., and R.W. Aldrich. 1999. Allosteric voltage gating of potassium channels II. *Mslo* channel gating charge movement in the absence of Ca^{2+}. *J. Gen. Physiol.* 114:305–336.

Horrigan, F.T., J. Cui, and R.W. Aldrich. 1999. Allosteric voltage gating of potassium channels. I. mSlo ionic currents in the absence of Ca^{+2}. *J. Gen. Physiol.* 114:277–304.

Ildefonse, M., and N. Bennett. 1991. Single-channel study of the cGMP-dependent conductance of retinal rods from incorporation of native vesicles into planar lipid bilayers. *J. Membr. Biol.* 123:133–147.

Ildefonse, M., S. Crouzy, and N. Bennett. 1993. Gating of retinal rod cation channel by different nucleotides: comparative study of unitary currents. *J. Membr. Biol.* 130:91–104.

Jan, L.Y., and Y.N. Jan. 1990. A superfamily of ion channels. *Nature.* 345:672.

Karlson, K.H., F. Ciampolillo-Bates, D.E. McCoy, N.L. Kizer, and B.A. Stanton. 1995. Cloning of a cGMP-gated cation channel from mouse kidney inner medullary collecting duct. *Biochim. Biophys. Acta.* 1236:197–200.

Karpen, J.W., R.L. Brown, L. Stryer, and D.A. Baylor. 1993. Interactions between divalent cations and the gating machinery of cyclic GMP–activated channels in salamander retinal rods. *J. Gen. Physiol.* 101:1–25.

Kaupp, U.B., T. Niidome, T. Tanabe, S. Terada, W. Bönigk, W. Stühmer, N.J. Cook, K. Kangawa, H. Matsuo, T. Hirose, et al. 1989. Primary structure and functional expression from complementary DNA of the rod photoreceptor cyclic GMP–gated channel. *Nature.* 342:762–766.

Kingston, P.A., F. Zufall, and C.J. Barnstable. 1996. Rat hippocampal neurons express genes for both rod retinal and olfactory cyclic nucleotide–gated channels: novel targets for cAMP/cGMP function. *Proc. Natl. Acad. Sci. USA.* 93:10440–10445.

Komatsu, H., I. Mori, J.S. Rhee, N. Akaike, and Y. Ohshima. 1996. Mutations in a cyclic nucleotide–gated channel lead to abnormal thermosensation and chemosensation in *C. elegans. Neuron.* 17: 707–718.

Kramer, R.H., E. Goulding, and S.A. Siegelbaum. 1994. Potassium channel inactivation peptide blocks cyclic nucleotide–gated channels by binding to the conserved pore domain. *Neuron.* 12: 655–662.

Lancet, D. 1986. Vertebrate olfactory reception. *Annu. Rev. Neurosci.* 9:329–355.

Liu, D.T., G.R. Tibbs, P. Paoletti, and S.A. Siegelbaum. 1998. Constraining ligand-binding site stoichiometry suggests that a cyclic nucleotide–gated channel is composed of two functional dimers. *Neuron.* 21:235–248.

Liu, D.T., G.R. Tibbs, and S.A. Siegelbaum. 1996. Subunit stoichiometry of cyclic nucleotide–gated channels and effects of subunit order on channel function. *Neuron.* 16:983–990.

Mannuzzu, L.M., M.M. Moronne, and E.Y. Isacoff. 1996. Direct physical measure of conformational rearrangement underlying potassium channel gating. *Science.* 271:213–216.

Marunaka, Y., A. Ohara, P. Matsumoto, and D.C. Eaton. 1991. Cyclic GMP–activated channel activity in renal epithelial cells (A6). *Biochim. Biophys. Acta.* 1070:152–156.

McLaren, A.D., and D. Shugar. 1964. Photochemistry of Proteins and Nucleic Acids. The MacMillan Co., New York, NY. 449 pp.

Middendorf, T.R., R.W. Aldrich, and D.A. Baylor. 2000. Modification of cyclic nucleotide–gated ion channels by ultraviolet light. *J. Gen. Physiol.* 116:277–252.

Misaka, T., Y. Kusakabe, Y. Emori, S. Arai, and K. Abe. 1998. Molecular cloning and taste bud-specific expression of a novel cyclic nucleotide–gated channel. *Ann. NY Acad. Sci.* 855:150–159.

Morrill, J.A., and R. MacKinnon. 1999. Isolation of a single carboxyl-carboxylate proton binding site in the pore of a cyclic nucleotide–gated channel. *J. Gen. Physiol.* 114:71–83.

Monod, J., J. Wyman, and J.P. Changeux. 1965. On the nature of allosteric transitions: a plausible model. *J. Mol. Biol.* 12:88–118.

Paoletti, P., E.C. Young, and S.A. Siegelbaum. 1999. C-Linker of cyclic nucleotide–gated channels controls coupling of ligand binding to channel gating. *J. Gen. Physiol.* 113:17–34.

Perozo, E., D.M. Cortes, and L.G. Cuello. 1998. Three-dimensional architecture and gating mechanism of a K^+ channel studied by EPR spectroscopy. *Nat. Struct. Biol.* 5:459–469.

Perozo, E., D.M. Cortes, and L.G. Cuello. 1999. Structural rearrangements underlying K^+-channel activation gating. *Science.* 285:73–78.

Picones, A., and J.I. Korenbrot. 1995. Spontaneous, ligand-independent activity of the cGMP-gated ion channels in cone photoreceptors of fish. *J. Physiol.* 485:699–714.

Ratcliffe, C.F., E.C. Conley, and W.J. Brammar. 1995. Distribution of cGMP-gated cation channel expression in bovine and porcine cardiovascular tissue. *Biochem. Soc. Trans.* 23:441S.

Rothberg, B.S., and K.L. Magleby. 1999. Gating kinetics of single large-conductance Ca^{2+}-activated K^+ channels in high Ca^{2+} suggest a two-tiered allosteric gating mechanism. *J. Gen. Physiol.* 114: 93–124.

Ruiz, M., R.L. Brown, Y. He, T.L. Haley, and J.W. Karpen. 1999. The single-channel dose–response relation is consistently steep for rod cyclic nucleotide–gated channels: implications for the interpretation of macroscopic dose–response relations. *Biochemistry.* 38:10642–10648.

Ruiz, M.L., and J.W. Karpen. 1997. Single cyclic nucleotide–gated channels locked in different ligand-bound states. *Nature.* 389: 389–392.

Ruiz, M.L., and J.W. Karpen. 1999. Opening mechanism of a cyclic nucleotide–gated channel based on analysis of single channels locked in each liganded state. *J. Gen. Physiol.* 113:873–895.

Schoppa, N.E., and F.J. Sigworth. 1998. Activation of *Shaker* potassium channels. III. An activation gating model for wild-type and V2 mutant channels. *J. Gen. Physiol.* 111:313–342.

Stern, J.H., H. Knutsson, and P.R. MacLeish. 1987. Divalent cations directly affect the conductance of excised patches of rod photoreceptor membrane. *Science.* 236:1674–1678.

Stryer, L. 1986. Cyclic GMP cascade of vision. *Annu. Rev. Neurosci.* 9:87–119.

Sunderman, E.R., and W.N. Zagotta. 1999. Mechanism of allosteric modulation of rod cyclic nucleotide–gated channels. *J. Gen. Physiol.* 113:601–620.

Taylor, W.R., and D.A. Baylor. 1995. Conductance and kinetics of single cGMP-activated channels in salamander rod outer segments. *J. Physiol.* 483:567–582.

Tibbs, G.R., E.H. Goulding, and S.A. Siegelbaum. 1997. Allosteric activation and tuning of ligand efficacy in cyclic-nucleotide–gated channels. *Nature.* 386:612–615.

Timpe, L.C., K.L. Jin, L. Puelles, and J.L. Rubenstein. 1999. Cyclic nucleotide–gated cation channel expression in embryonic chick brain. *Brain Res. Mol. Brain Res.* 66:175–178.

Varnum, M.D., K.D. Black, and W.N. Zagotta. 1995. Molecular mechanism for ligand discrimination of cyclic nucleotide–gated channels. *Neuron.* 15:619–625.

Varnum, M.D., and W.N. Zagotta. 1996. Subunit interactions in the activation of cyclic nucleotide–gated ion channels. *Biophys. J.* 70: 2667–2679.

Varnum, M.D., and W.N. Zagotta. 1997. Interdomain interactions underlying activation of cyclic nucleotide–gated channels. *Science.* 278:110–113.

Vladimirov, Y.A., D.I. Roshchupkin, and E.E. Fesenko. 1970. Photochemical reactions in amino acid residues and inactivation of enzymes during U.V.-irradiation. A review. *Photochem. Photobiol.* 11: 227–246.

Weyand, I., M. Godde, S. Frings, J. Weiner, F. Müller, W. Altenhofen, H. Hatt, and U.B. Kaupp. 1994. Cloning and functional expression of a cyclic-nucleotide–gated channel from mammalian sperm. *Nature.* 368:859–863.

Yao, X., A.S. Segal, P. Welling, X. Zhang, C.M. McNicholas, D. Engel, E.L. Boulpaep, and G.V. Desir. 1995. Primary structure and functional expression of a cGMP-gated potassium channel. *Proc. Natl. Acad. Sci. USA.* 92:11711–11715.

Yau, K.W., and D.A. Baylor. 1989. Cyclic GMP–activated conduc-

tance of retinal photoreceptor cells. *Annu. Rev. Neurosci.* 12:289–327.

Zagotta, W.N., T. Hoshi, and R.W. Aldrich. 1994. *Shaker* potassium channel gating. III: Evaluation of kinetic models for activation. *J. Gen. Physiol.* 103:321–362.

Zhang, Q., S. Pearce-Kelling, G.M. Acland, G.D. Aguirre, and K. Ray. 1997. Canine rod photoreceptor cGMP-gated channel protein alpha-subunit: studies on the expression of the gene and characterization of the cDNA. *Exp. Eye Res.* 65:301–309.

Zimmerman, A.L., and D.A. Baylor. 1992. Cation interactions within the cyclic GMP-activated channel of retinal rods from the tiger salamander. *J. Physiol.* 449:759–783.

Zong, X., H. Zucker, F. Hofmann, and M. Biel. 1998. Three amino acids in the C-linker are major determinants of gating in cyclic nucleotide–gated channels. *EMBO (Eur. Mol. Biol. Organ.) J.* 17: 353–362.

Zufall, F., S. Firestein, and G.M. Shepherd. 1994. Cyclic nucleotide–gated ion channels and sensory transduction in olfactory receptor neurons. *Annu. Rev. Biophys. Biomol. Struct.* 23:577–607.